A Report for . . .

EVALUATION OF THE BREADBOARD MICROWAVE METEROLOGICAL RADIOMETER AND SCANNING ANTENNA

SGC 939R-7

SPACE GENERAL TIRE GENERAL

EVALUATION OF THE BREADBOARD MICROWAVE METEROLOGICAL RADIOMETER AND SCANNING ANTENNA

March 15, 1967

MEMORANDUM TECHNICAL REPORT

SGG-939R-7 END

by

J. J. Kirwan
P. R. Jordan
R. Greenwood

Contract No. NAS 5-9680

H. G. Pascalar, Manager
Surveillance and Reconnaissance
Systems Division

G. Oister
Program Manager

Prepared by

SPACE-GENERAL CORPORATION
9200 East Flair Drive
El Monte, California

for

GODDARD SPACE FLIGHT CENTER
Greenbelt, Maryland

CONTENTS

ILLUSTRATIONS

Section 1

INTRODUCTION

The primary objective of this report is to summarize the results of measurements which were performed on the Nimbus breadboard electronic scanning antenna array. This series of measurements was intended primarily to establish the radiometric beam efficiency and to measure the dissipative loss of the Nimbus array over its range of scan angles, $\pm 50^{o}$. Also, it was desired to quantitatively relate the measured radiometric temperature of an object filling the main beam of the antenna.

Since the radiometer receiver had been accurately calibrated for absolute temperature measurements using the cold load bench test set (see Appendixes A and B), it was the best available instrument for performing the antenna measurement and, also, provided for an overall system functional checkout of the breadboard model.

These measurements were performed at Table Mountain, California, at an altitude of 7200 feet, thus minimizing the atmospheric absorption contributions to the zenith sky temperatures. A photograph of the test site is shown in Figure 1-1.

Details of the theory behind the measurements and of how the measurements were actually performed are discussed in Sections 2 and 3. The results and conclusions of the measurements are discussed in Sections 4 and 5, respectively.

Appendixes A, B and C describe the calibration of the radiometer, the cryogenic bench test site and the zenith sky temperature. Appendix D discusses the sun drift curves which were obtained by allowing the sun to drift through the antenna response, i.e., the antenna pattern.

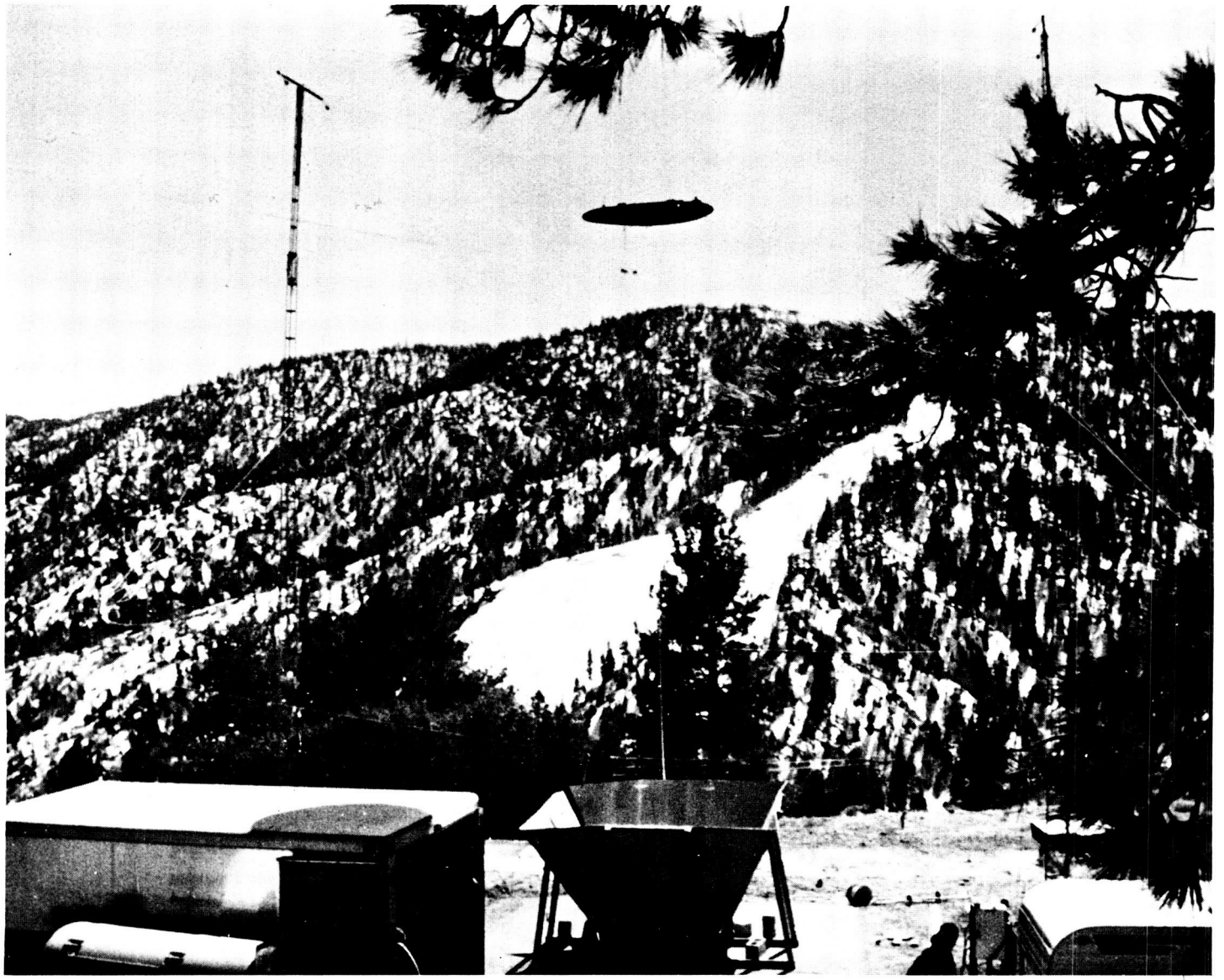

939/044

Figure 1-1. Photo of Test Site at Table Mountain

Section 2

ANTENNA LOSS AND EFFICIENCY MEASUREMENT TECHNIQUES

2.1 INSERTION LOSS AND EFFICIENCY EQUATIONS

The objectives of this series of tests were to establish the radiometric efficiency of the antenna array and to quantitatively relate the radiometric temperature at the antenna output to the brightness temperature of an object filling the antenna beam. An ideal antenna is one which receives all of its energy from the primary beam (i.e., side lobes = 0) and transmits all of this energy to its output. Practical antennas diverge from this ideal in that, as a consequence of side lobes, the power received in the main beam is reduced. For a given incident power from a source completely subtended by the main beam, the ratio of the power received with a given antenna compared to the incident power will be referred to here as the radiometric beam efficiency of the antenna. The sum of radiation received from objects intercepted by the side lobes adds an additional power output to the antenna output which is termined radiometric background temperature. Dissipative loss occurring within the antenna and associated feed structures attenuates both the main beam and side lobe components of the received radiation and adds a reradiation component to the total power available at the antenna output port. Thus, the power output of a practical receiving antenna may be described in terms of two components of incident radiation, the antenna dissipative insertion loss of the antenna, the antenna beam efficiency, and an associated reradiation component.

List of Definitions

P_{im} = power incident from main beam

P_{is} = total incident power from side lobes

E = antenna main beam efficiency

L_a = antenna dissipative insertion loss

List of Definitions (Continued)

P_{rm} = power input to receiver from main beam

P_{rs} = power input to receiver from side lobes

P_t = antenna loss power component

T_{im}, T_{is} = radiometric antenna brightness temperatures

T_z = zenith sky temperature

T_R = radiometer output temperature

t = thermal temperature of antenna

t_d = thermal temperature of absorbing disk

k = Boltzman's constant

B = receiver predetection bandwidth

The three components of power available at the output port to the receiver are (see list of definitions):

a. The main lobe component $P_{rm} = \frac{EP_{im}}{L_a}$

b. The side lobe component $P_{rs} = \frac{P_{is}}{L_a} (1 - E)$

c. The antenna loss reradiation component $P_t = \left(\frac{L_a - 1}{L_a}\right) t$

These power components may be related to radiometric brightness temperatures of the objects in the main and side lobes and to the thermal temperature of the dissipative elements in the antenna structure. It is assumed that the main beam observes a uniform brightness temperature, T_{im}, and that all of the side lobes observe a uniform brightness temperature, T_{is}, and that the antenna loss elements have a thermal temperature, t. The total power available to a receiver at the antenna port is, then:

$$P_\Sigma = \frac{E}{L_a} P_{im} + P_{is} \frac{(1 - E)}{L_a} + P_t$$

or

$$P_\Sigma = kB \left[\frac{E T_{im}}{L_a} + \frac{(1 - E)}{L_a} T_{is} + \left(\frac{L_a - 1}{L_a} \right) t \right]$$

It will be assumed that, within the bandwidth B, the antenna characteristics are initially uniform. Furthermore, it is assumed that within this bandwidth both the antenna and the receiver input are sufficiently well impedance-matched to the interconnecting transmission line so that any intervening insertion loss is purely dissipative, i.e., negligible power reflection.

The radiometric temperature of the antenna T_R output is, thus, given by

$$T_R = \frac{P_\Sigma}{kB} = \frac{E}{L_a} T_{im} + \left(\frac{(1 - E)}{L_a} \right) T_{is} + \left(\frac{L_a - 1}{L_a} \right) t$$

The primary objectives of the measurements that were conducted at Table Mountain were to accurately ascertain the values of E and L_a using this equation.

The antenna is a two-dimensional planar array which is electronically scanned over a range of $\pm 50^\circ$ in approximately 2.5° steps. Thus, it was necessary to determine the values of L_a and E at a sufficient number of angular portions within this range to permit an accurate determination of their variation as a function of scan angle.

In the following test procedures the radiometer itself is assumed to be calibrated sufficiently well to allow absolute temperature measurements. The calibration of the radiometer is exclusive of the antenna and is described in Appendix A.

2.2 BASIC TESTING PRINCIPLES

The principles underlying the tests and reasoning leading to the particular test approach will now briefly be discussed prior to their detailed description.

From the equation for T_R it is apparent that if the incident temperatures T_{is} and T_{im} were both zero, then a measurement of T_R by the radiometer and t by a precision thermistor would permit L_a to be computed as

$$L_a = \frac{t}{t - T_R}$$

Although zero values for T_{im} and T_{is} are impossible, since the minimum radiometric brightness temperatures available for the antenna are limited by atmospheric absorption at zenith and the isotropic universal background radiation, atmospheric absorption can be minimized by locating at a relatively high elevation where water vapor absorption is greatly reduced. For this reason, Table Mountain with an elevation of 7200 feet was selected as the test site. Under clear sky conditions the zenith sky temperature observed was approximately $8^{\circ}K$ and ascertainable to an accuracy of $\pm 2^{\circ}K$.

If both T_{is} and T_{im} could be made approximately equal to the zenith temperature, T_z, then the equation for T_{at} is

$$T_R = \left[\frac{E}{L_a} + \frac{(1 - E)}{L_a}\right] T_z + \left(\frac{L_a - 1}{L_a}\right) t$$

Then

$$L_a = \frac{t - T_z}{t - T_R}$$

In practice, T_{is} and T_{im} can be made nearly equal by placing a reflecting surface at the back and flaring out along the sides of the antenna so that the side lobes are reflected into a cone centered at zenith. (See Figures 2-1 and 2-2).

Under clear sky conditions the atmospheric absorption varies only very slightly for small angles from the zenith and, thus, $T_{is} \simeq T_{im}$. The actual values of T_z used during the course of these measurements were calculated as discussed in Appendix C. T_z can also be determined from the antenna temperatures obtained by observing the radiometer output temperature as a function of zenith angle. Under these conditions, the predominant portion of T_R will be due to the reradiation from the insertion loss of the array antenna.

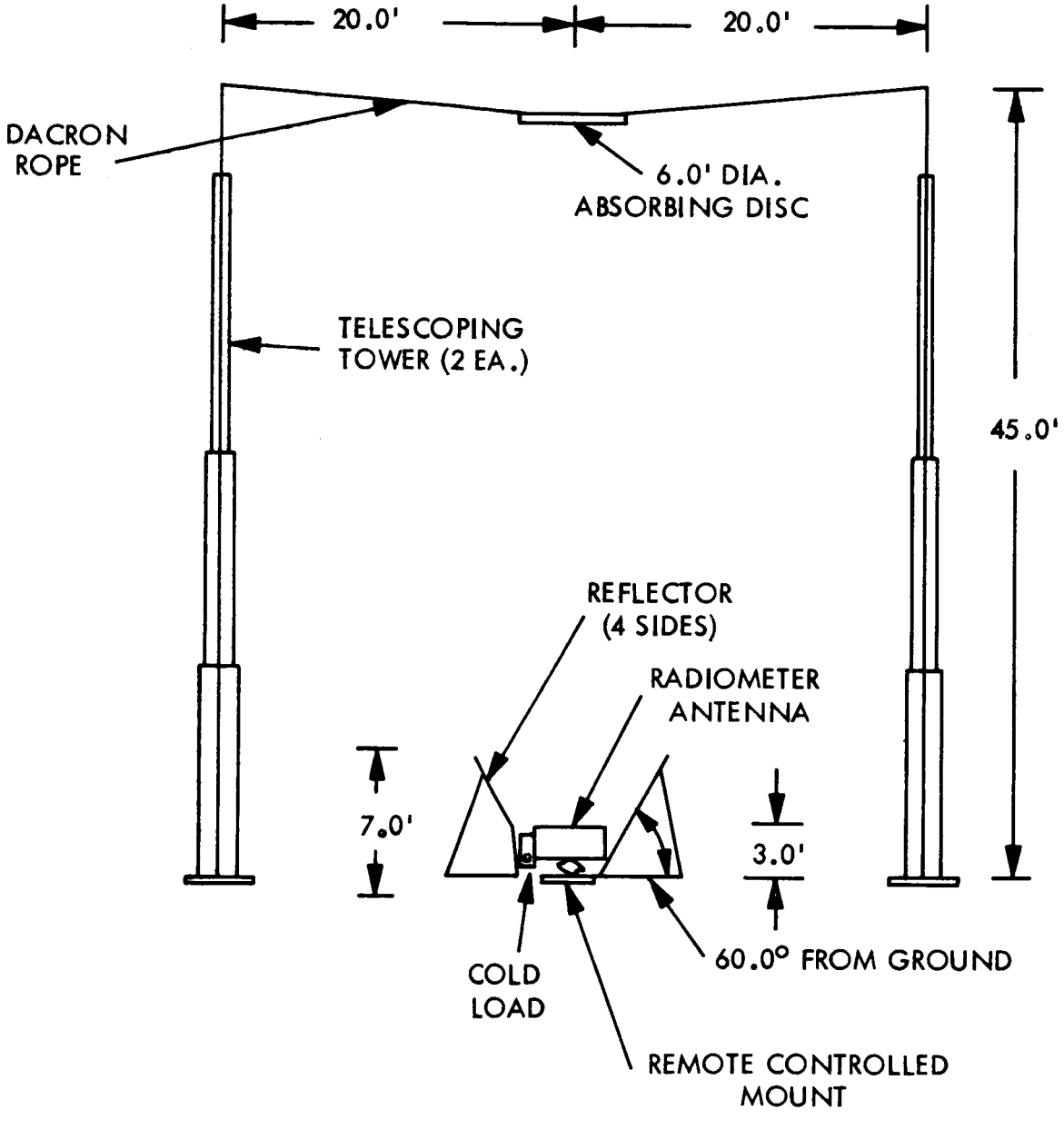

Figure 2-1. Reflector Geometry

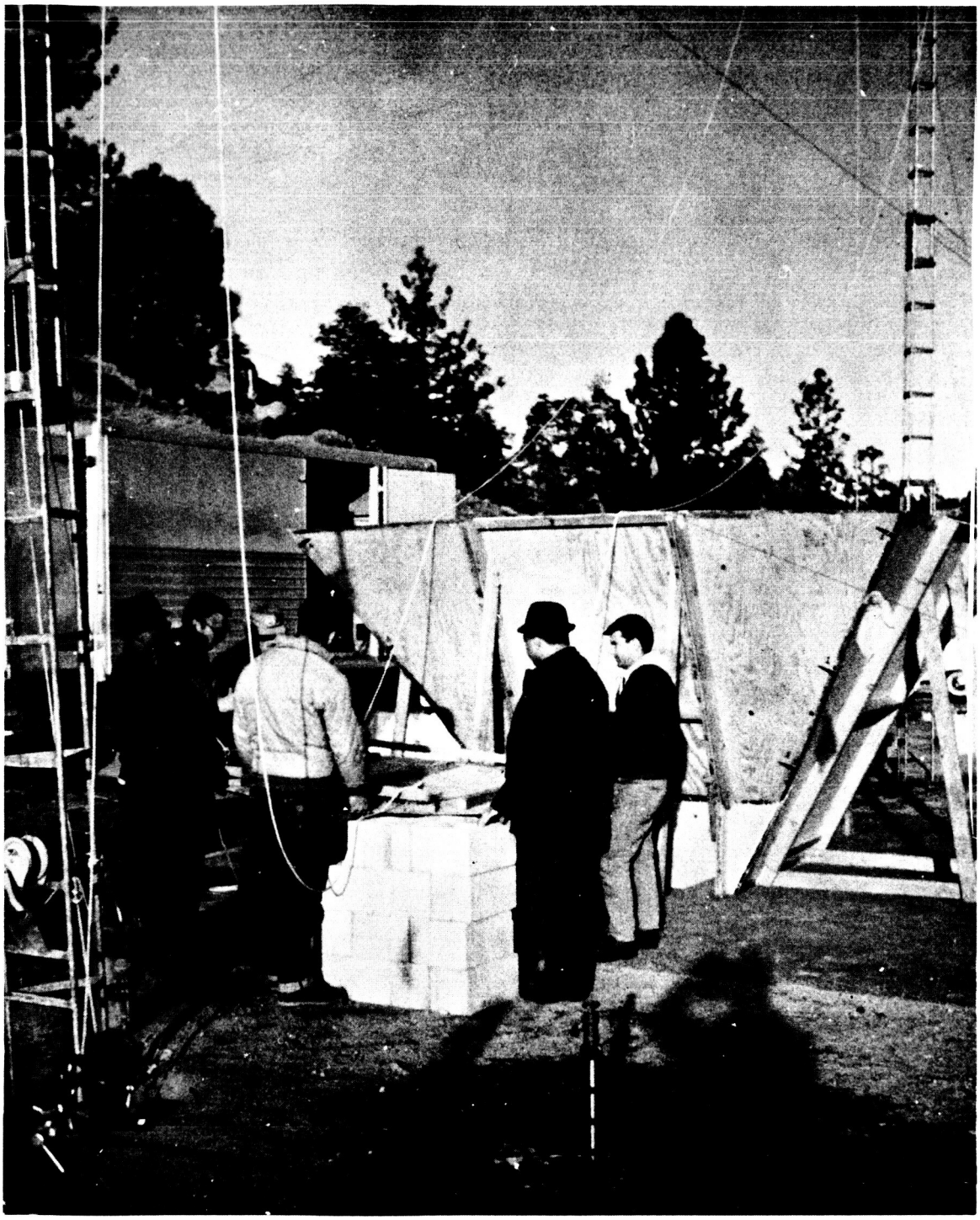

939/040

Figure 2-2. Reflectors Positioned Around Antenna Array

The antenna loss, L_a, was measured for different thermal temperatures of the antenna at 0^o beam position. The loss, L_a, should be somewhat independent of the thermal temperature of the antenna. The thermal temperature range that was obtained is 4^oC to 35^oC by taking advantage of the natural ambient temperature range and using electrical heaters.

The next step is to find the efficiency E of the antenna. This was accomplished by placing a disk-shaped, black-body target in the main lobe of the antenna pattern. The disk was shaped to fill the main lobe of the antenna out to the null points at a distance of approximately 35 feet above the antenna. (See Figures 2-1 and 2-3). The thermal temperature of the disk, T_d, was monitored by a calibrated thermistor. By maximizing the radiometer output signal, the disk was centered in the beam. Since the disk fills the beam at the null points, the accuracy of the measurement is not a strong function of the disk centering.

The antenna output temperature, T_R, is now given by

$$T_R = \frac{E\, t_d}{L_a} + \frac{(1 - E)\, T_z}{L_a} + \frac{t(L_a - 1)}{L_a}$$

Since the efficiency, E, of the antenna is known from the antenna pattern measurements to be near 0.9, the loss $L_a \simeq 2$ dB, and $T_z \approx 8^oK$, the second term in the above equation is $\approx \frac{1}{2}^oK$. The loss, L_a, is known from the previous measurement, and the thermal temperatures of the disk, t_d, and the antenna, t, are monitored. The antenna radiometric output temperature is measured and from the above formula the efficiency calculated. Section 3 contains a description of the test procedure which was followed during the course of these measurements.

2.3 SKY HORN MEASUREMENT

The antenna loss at several beam positions may also be measured by comparing a standard gain horn (Scientific Atlanta, Model No. 12-18S/N 36) with the antenna array. This was done at two beam positions by connecting the standard gain horn and a precision variable attenuator on the calibration port and the antenna array on the antenna port (see Figure 2-4). Then the attenuator was positioned so as to present equal readings on the calibration readout and antenna readout. This was performed at both 0^o and $+16^o$ beam positions.

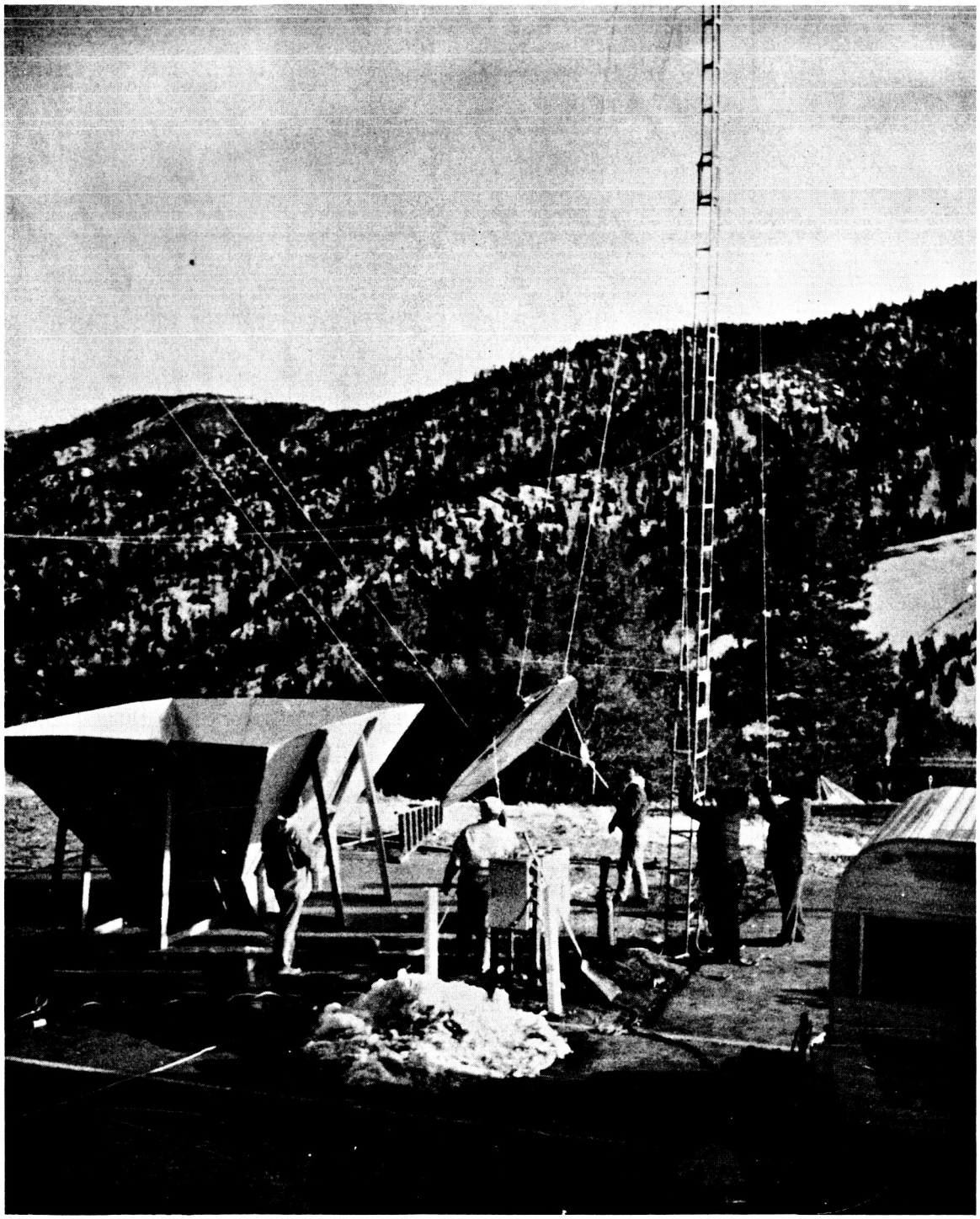

939/048

Figure 2-3. Absorbing Disks Positioned Above Antenna Array

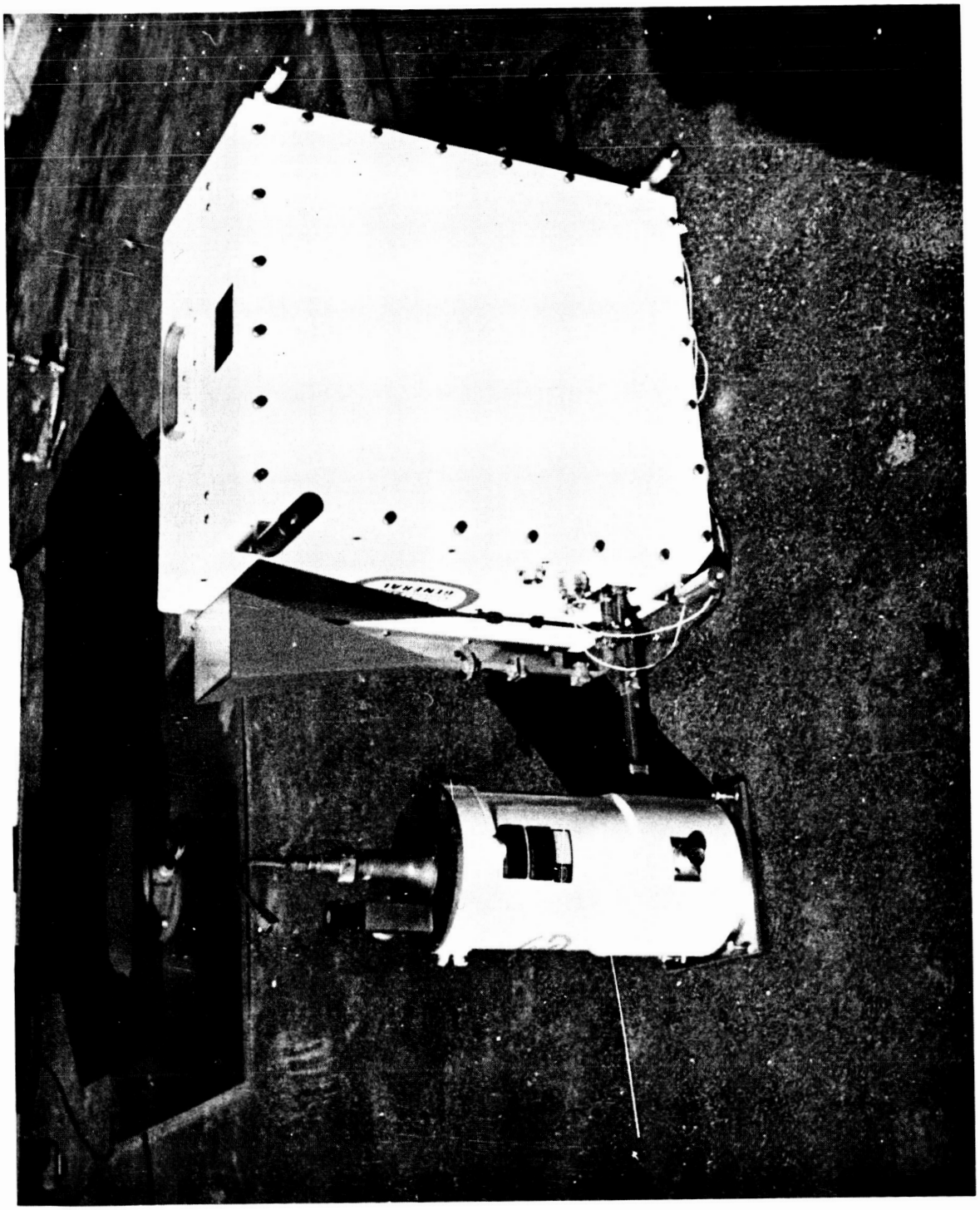

939/042

Figure 2-4. Standard Gain Horn Connected to Calibration Port

Section 3

TEST PROCEDURE

3.1 STEPS FOLLOWED DURING TESTS

1. The radiometer was recalibrated with the cryogenic bench test set on arriving at Table Mountain before proceeding with the tests of the antenna. A calibration curve is shown in Figure 3-1 for liquid nitrogen filling the bench test set cryoflask.

2. The radiometer and antenna were mounted on a pedestal with the cryogenic load attached to the cold reference waveguide port (see Figure 3-2).

3. The antenna coil currents were set to produce the 0° beam position and the antenna was mechanically oriented to point the beam at the zenith. A measurement was made with no reflectors to get an estimate of the energy in the back lobes.

4. The reflectors were placed around the radiometer to shield the antenna from the ground.

5. The radiometer output was recorded for five minutes by means of the digital printer, both with and without a polyfoam enclosure to measure the effect of this enclosure.

6. During the measurement of Step 5, the following parameters were also recorded:

   a. Ambient air temperature

   b. Humidity

   c. Barometric pressure

   d. Sky cover

   e. Thermal temperature of antenna at center and two edges of array

   f. Temperatures within the antenna and radiometer enclosure

   g. Temperature distribution along cold load feed line

7. From the data of Steps 5 and 6, the antenna loss in dB was calculated.

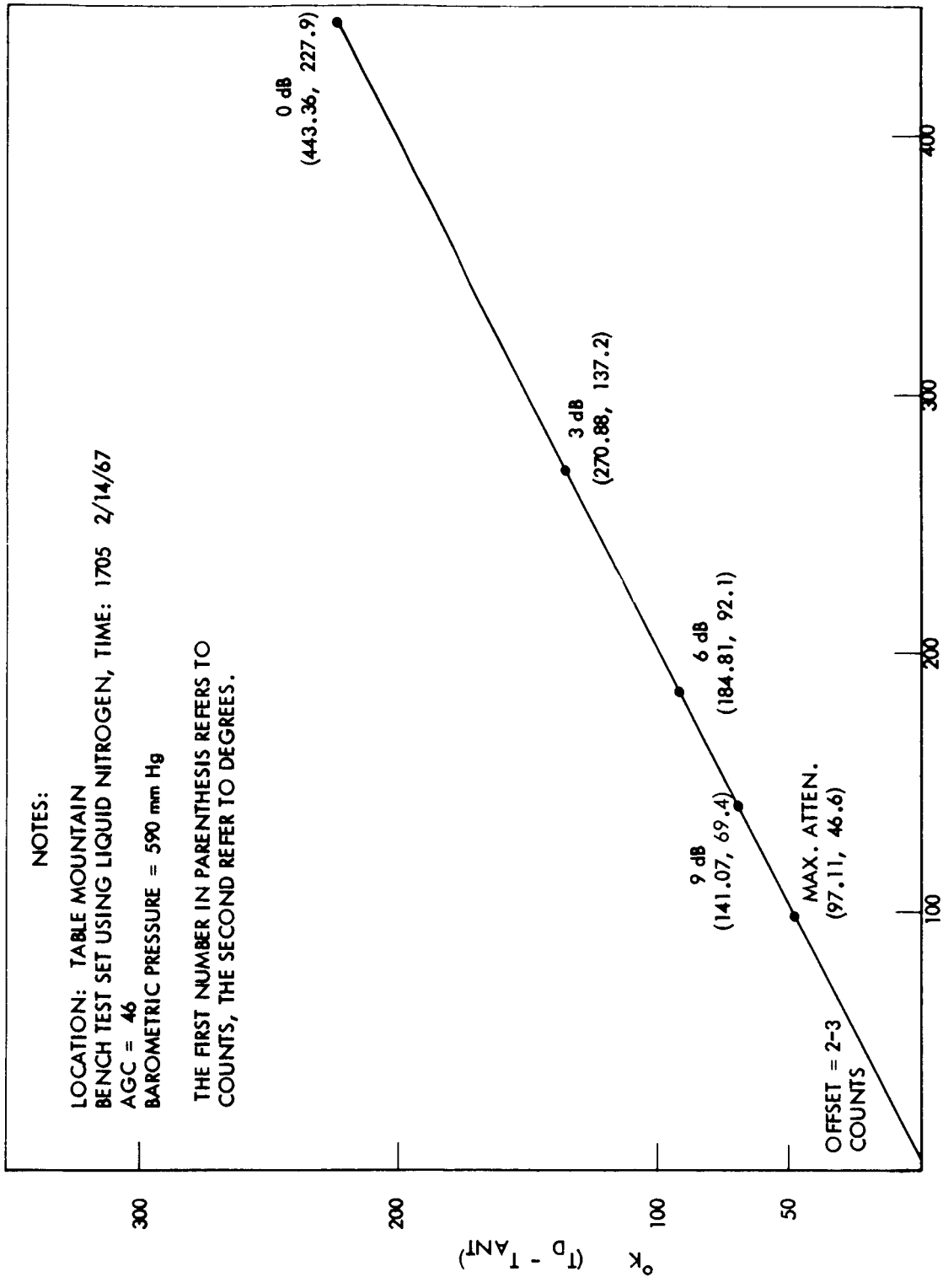

Figure 3-1. Calibration Curve of Radiometer

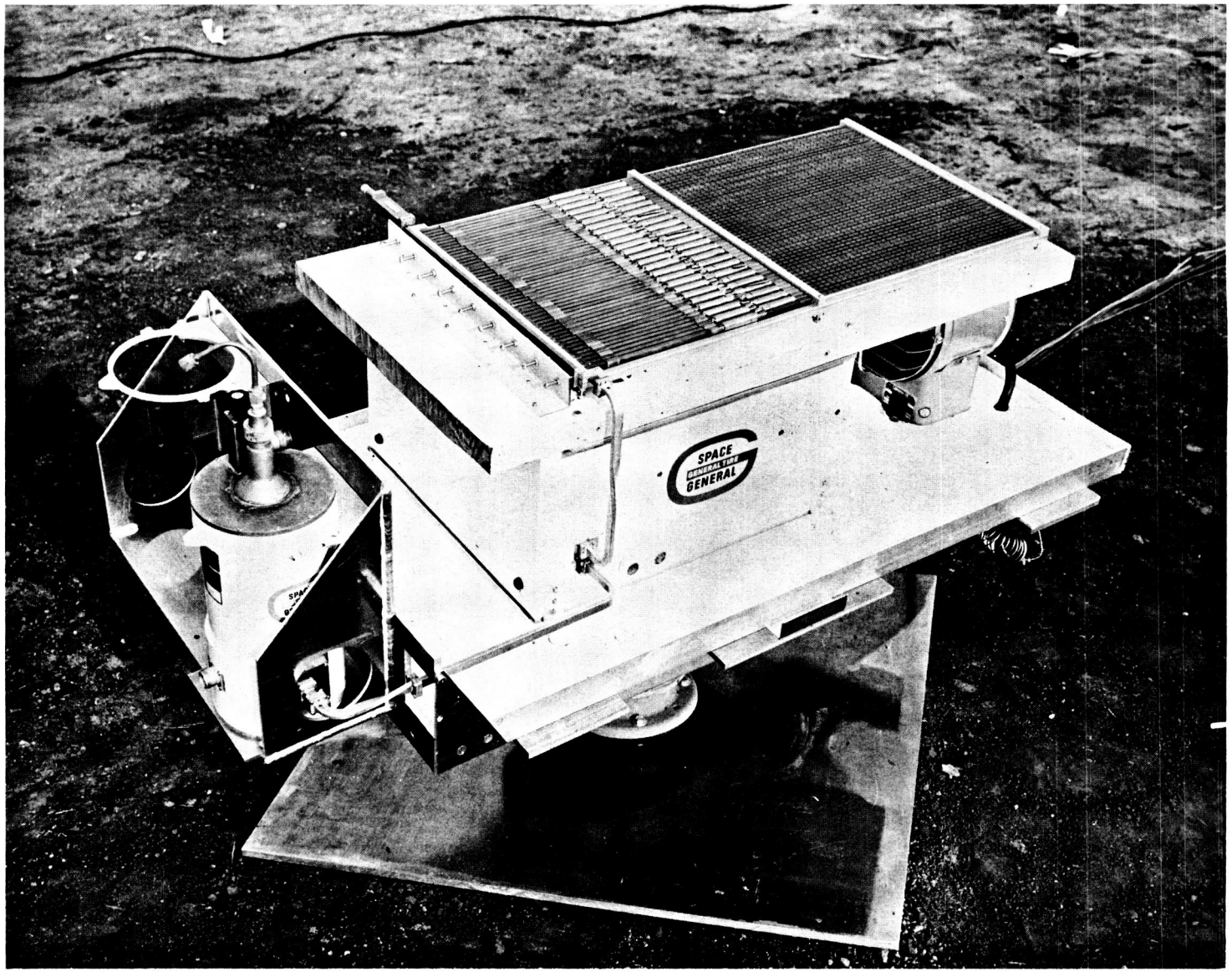

939/022

Figure 3-2. Cold Reference Load and Radiometer

8. By means of towers a disk of absorbing material was positioned over the antenna so that it filled the main lobe out to the null points. (See Figure 3-3.) The height of the disk above the antenna was approximately thirty-five feet.

9. The radiometer output was then recorded for five minutes by means of the digital printer.

10. During the measurement of Step 9, the following parameters were also recorded:

    a. Ambient air temperature

    b. Humidity

    c. Barometric pressure

    d. Sky cover

    e. Thermal temperature of antenna at center and two edges of array

    f. Temperatures within the antenna and radiometer enclosure

    g. Thermal temperature of absorbing disk

    h. Temperature distribution along the cold reference load feed line

    i. Height of disk above antenna

    j. Motion of disk (estimated)

11. The disk's position was then moved while observing the radiometer output to maximize the temperature recorded at the output of the radiometer, and data taken, as discussed in Steps 9 and 10.

12. From the measurements in Steps 10 and 11 and the antenna loss calculated in Step 7, the percentage of energy in the main lobe of the antenna was calculated.

13. The antenna coil currents were then set to position the antenna at other beam positions and the measurements described in Steps 2 through 12 repeated. In all cases the antenna was tilted mechanically so that the main beam pointed at the zenith.

14. The above measurements were repeated for the scan angles of approximately -45, -31, -16, +16, +31, and +45, in that order, repeating the procedure in Steps 5 through 12.

939/043

Figure 3-3. Absorbing Disk Over Antenna Array

15. From the above measurements, the antenna loss and percentage of energy in the main lobe of the antenna have been determined for the scan angles of -45°, -31°, -16°, 0°, $+16^{\circ}$, $+31^{\circ}$, $+15^{\circ}$, and this data was compared to the antenna loss and beam efficiency obtained from the antenna pattern measurements and the antenna loss obtained from the measurements of the loss of individual components.

16. The standard gain horn was then connected to the cold reference load port through a precision variable attenuator and some additional waveguide. The attenuator was set on 0 dB setting and the radiometer output was then recorded.

17. Comparison of the calibration output and antenna output readings were made. Additional attenuation was inserted via the variable attenuator until the calibration output and antenna output readings were nearly equal.

18. The connecting line from the standard gain horn, including the precision attenuator, was then estimated to have 2.5 dB loss.

Section 4

TEST RESULTS

The two measured antenna parameters of major importance are the antenna insertion loss and beam efficiency. Secondary quantities measured while at Table Mountain were the sky zenith temperature and the temperature of the sun. These measurements also provide some degree of correlation on the antenna loss. Sample calculations of the insertion loss and beam efficiency are included below. Table 4-1 lists these quantities as well as those values obtained from the integration of antenna patterns as measured at the SGC antenna range.

4.1 INSERTION LOSS AND BEAM EFFICIENCY

The equation for the insertion loss was presented in Section 2. This equation was derived assuming that all the incident energy from the main antenna beam as well as from the side lobes and back lobes of the antenna is from the sky. This condition is presumably established by placing a reflecting surface at the back and flaring out along the sides of the antenna as shown in Figure 2-1. To determine the reflector effectiveness and/or the back lobe level, a measurement of the sky temperature was performed at 0^{o} beam position, both with and without the reflectors. A comparison of the resulting antenna temperatures shows that the total energy in the back lobes is less than 0.5 percent and that the reflectors do some good, although if they were not used only small errors would result.

Next, several measurements were performed, both with and without the polyfoam enclosure which housed the receiver and antenna. This measurement resulted in the somewhat intriguing fact that the antenna loss was slightly less with the enclosure on than with it removed. This may be attributed to the fact that antenna reflection losses, although thought to be small enough to be ignored, were measurable with such a sensitive receiver. The effect of the polyfoam is to improve the impedance match from a VSWR value

Table 4-1

TEST RESULTS

Beam Position	Insertion Loss (dB)	Beam Efficiency Measurements (%)	Antenna Thermal Temperature °C	T_z, Calculation °K	Reference Load	Beam Efficiency Calculation (%)
0°	2.66	-	+ 4	7	Cold Load, N_2	88.9**
0°	2.60	86.3	+14	8	Cold Load, N_2	
0°	2.52	87.3	+17.1	7	Cold Load, N_2	
0°	2.66	-	+18.4	7	Ref. Horn	
0°	2.49	-	+19.1	7	Cold Load, N_2	
0°	2.57	89	+28.9	6	Cold Load, N_2	
0°	2.54	72*	+35.7	8	Cold Load, N_2	
0° Avg.	$2.57^{+.09}_{-.08}$					
+16°	2.50	90	+37.2	6.5	Cold Load, N_2	
+31°	2.54	80.8*	+12.4	9	Cold Load, N_2	93
+31°	2.60	90.5	+18.1	7	Ref. Horn	
+31°	2.69	-	+19.4	7	Ref. Horn	
+31° Avg.	$2.61^{+.08}_{-.07}$					
+45°	2.76	86	+18.5	8.5	Ref. Horn	
+45°	2.64	82	+16.3	8.5	Cold Load, N_2	
+45° Avg.	2.70 ± .06					
Fail Safe	2.46	89.5	23.1	6.5	Cold Load, N_2	
Fail Safe	2.58		18.5	7	Ref. Horn	
Fail Safe, Avg	2.52 ± .06					
-16°	2.52	90.5	+35	6	Cold Load, N_2	88.6
-31°	2.57	81	+ 4.7	8	Cold Load, N_2	
-45°	2.79	80	- 1	7	Cold Load, N_2	
-45°	2.74	78.6	+35.7	7	Cold Load, N_2	
-45° Avg.	2.765 ± .025					

NOTES:
* The disk did not fill the main beam of the antenna during these measurements.
**Beam efficiencies were not calculated for all scan angles.

of, say, 1.2 to a value of 1.1. These numbers are not quoted measured values but are only mentioned here to show the relative values of impedance match under discussion. The resulting antenna insertion loss difference, with and without the enclosure, is on the order of .046 dB and will be neglected since the antenna temperature difference for the two cases was on the order of $1^{\circ}K$.

Table 4-1 lists the measured antenna insertion losses and measured beam efficiencies when using the radiometer receiver. Also included is the thermal temperature of the antenna and the assumed value of T_z for each individual measurement. A column is also provided which lists the beam efficiency calculated when using individual antenna patterns taken at the center operating frequency of the antenna. Several of the measurements were performed using a standard gain horn as the calibration load, while the majority were performed using a cryogenic load cooled to the boiling point of liquid nitrogen. Reasonably good correlation was obtained between the two conditions. A sample calculation of the insertion loss and beam efficiency are shown below for a beam position of $+16.2^{\circ}$. The loss is given by the equation

$$L_a = \frac{t - T_z}{t - T_R}$$

where all quantities were defined previously. Values of t, T_z, and T_R used are

$t = 311.2^{\circ}K$ (a measured thermal antenna temperature)

$T_z = 6.5^{\circ}K$ (a calculated zenith sky temperature)

$T_R = 150^{\circ}K$ (a measured radiometric antenna temperature)

Thus,

$$L_a = \frac{311.2 - 6.5}{311.2 - 150} = 1.890 = 2.765 \text{ dB}$$

Included in this loss is a waveguide connection from the antenna port to the radiometer input. This waveguide has a measured loss of .266 dB and must be subtracted from the L_a value obtained above, thus yielding a value of $L_a' = 2.50$ dB. Beam efficiency is given by the equation

$$E = \frac{L_a T_R - T_z - t\left(L_a - 1\right)}{td - T_z}$$

For the above insertion loss, the following values of temperature were used:

$t = 310.3^{\circ}K$ (a measured thermal antenna temperature)

$t_d = 290.3^{\circ}K$ (a measured absorbing disk temperature)

$T_z = 6.9^{\circ}K$ (a calculated zenith sky temperature)

$T_R = 283.5^{\circ}K$ (measured radiometric antenna temperature)

$$E = \frac{1.890\,(283.5) - 6.5 - 310.3\,(.890)}{290.3 - 6.5} = 90\%$$

Notice that the insertion loss of the waveguide connection from the antenna port to the radiometer input is included in this calculation. This is necessary because the radiometric antenna temperature is measured at the radiometer input port. This input port is the reference plane for all measured radiometric data.

4.2 ERRORS IN INSERTION LOSS DUE TO UNCERTAINTIES IN TEMPERATURE MEASUREMENTS

The expression for antenna insertion loss contains three temperature terms, two of which are radiometric temperatures while the other is a thermal temperature. Uncertainties in the measurement or assumed values of these quantities result in an overall uncertainty or error in values of insertion loss. The maximum uncertainty in L is given by

$$\Delta L = \frac{|\Delta T_z|}{t - T_R} + \frac{|T_z - T_R||\Delta t|}{\left(t - T_R\right)^2} + \frac{|t - T_z||\Delta T_R|}{\left(t - T_R\right)^2}$$

Typical values of these quantities are:

$t \simeq 270 - 300^{\circ}K \pm .5^{\circ}K$

$T_R \simeq 140 - 150^{\circ}K \pm 1^{\circ}K$

$T_z \simeq 6 - 8^{\circ}K \pm 2^{\circ}K$

Under the worst combination of these values of temperature the maximum uncertainty is:

$$\Delta L = \frac{2}{130} + \frac{144(.5)}{(130)^2} + \frac{264(1)}{(130)^2}$$

$$= .0154 + .00435 + .0161 = .036$$

For $L = 1.9$

$$\frac{\Delta L}{L} = \frac{.036}{1.9} = 1.9\% = .18 \text{ dB error, maximum}$$

This is the maximum possible error. The rms error is probably on the order of ± .06 dB.

4.3 BEAM EFFICIENCY ERRORS

The equation for beam efficiency was derived in Section 2. In a different form it is:

$$E = \frac{L_a T_R - T_z - t\left(L_a - 1\right)}{t_d - T_z}$$

Errors in the temperature measurements, both thermal and radiometric, and in the antenna insertion loss, result in uncertainties in the antenna efficiency measurement. It will be assumed here that errors in filling the main beam with the disk are negligible compared to other errors.

The total maximum error in measuring E is the sum of the errors in measuring each of the quantities in the above expression for E. These will be discussed separately below.

The uncertainty in E due to uncertainties in L_a are:

$$\Delta E_L = \frac{|T_R - t|\Delta L|}{td - T_z}$$

This term will add the most uncertainty to the total, since the uncertainty in L is somewhat large for this measurement. For the typical values

which occur, i.e., $T_R = 260^oK$, $t = 290^oK$, $td = 290^oK$, $T_z = 9^oK$ and for the value of $\Delta L = .028$ calculated previously ΔE_L equals $\simeq 3\%$.

The following typical values for the other variables in the equation are:

$$L_a = 1.9,\ T_R = 260^oK,\ T_z = 9^oK,\ t = 290^oK,\ td = 290$$

$$\Delta L_a = .028\ \Delta T_R = 1^oK\ \Delta T_z = 1^oK\ \Delta t = .5^oK\ \Delta td = 2^oK$$

The uncertainty in E due to uncertainty in T_R is given by

$$\Delta E_{TR} = \frac{L_a\ |\Delta T_R|}{t_d - T_z} = .675\%$$

The uncertainty in E due to uncertainty in T_z is:

$$\Delta E_{Tz} = \frac{|t_d - T_z|\,|\Delta T_z| - |L_a\ T_R - T_z - t(L_a - 1)|\,|\Delta T_z|}{(t_d - T_z)^2} = .07\%$$

The uncertainty in E due to the uncertainty is t is

$$\Delta E_t = \frac{|L_a - 1|\,|\Delta t|}{t_d - T_z} = .16\%$$

and the uncertainty E due to the uncertainty in td

$$\Delta E_{td} = \frac{|L_a\ T_R - T_z - t\,|L_a - 1||\,td\,|}{td - T_z^{\,2}} = .56\%$$

It is interesting to note that the uncertainty in the disk temperature, although somewhat large, does not contribute appreciably to the overall uncertainty. The total <u>maximum</u> uncertainty is the sum of these, or

$$\Delta E_\Sigma = 4.465\%$$

The rms error is on the order of ± 1.5%.

4.3.1 SKY HORN MEASUREMENT RESULTS

When the standard gain horn and attenuator were connected as the calibration load, the attenuator was positioned to obtain equal output readings on the antenna output and calibration output. Fairly good correlation was obtained between this rough insertion loss measurement and the method described in Section 2. For the two beam positions used the results are as follows:

	Beam Position	
Insertion Loss of Cold Horn Waveguide Run	+16.2°	0°
Precision Attenuation Reading (meas.)	1.55 dB	1.60
Residual Loss at 0 dB (meas.)	.46 dB	.46
Loss of w/g (meas.)	.21 dB	.21
Loss of Standard Gain Horn (est.)	.20 dB	.20
	2.42 dB	2.47 dB
Less the Loss of Antenna Feed	-.27	-.27
Total Loss, Approx.	2.15	2.20

These values are approximately .25 dB lower than obtained by the more exact method although they indicate that the antenna loss is indeed greater than 2 dB. This measurement is interesting in that no value of the zenith temperature and no value of the calibration port (cold reference load) temperature are required.

4.4 SKY TEMPERATURE MEASUREMENT

A measurement of the sky temperature was performed at an electrical beam position of + 31.2°. The antenna was tilted mechanically to observe five different angles from the zenith. The sky temperature is given by:

$$T_z = t - L_a \left(t - T_R\right)$$

where all terms have previously been defined. A table of these measurements is given below:

Angle from Zenith	T_z
$+11^{\circ}$	$8.08^{\circ}K$
$+31^{\circ}$	$9.92^{\circ}K$
$+45^{\circ}$	$10.89^{\circ}K$
$+60^{\circ}$	$16.43^{\circ}K$
$+76^{\circ}$	$27.58^{\circ}K$

The error in this measurement can be quite pronounced for such a large antenna loss, although the calculated value for this measurement was $7.9^{\circ}K$ at zenith position (0°). Due to the error in antenna loss alone the uncertainty in T_z is typically $3^{\circ}K$, not a small number in comparison.

Calculated values of the sky temperature have been made for this altitude (pressure), humidity and ambient temperature utilizing several well-known references. The calculated values of from 6 - $9^{\circ}K$ agrees quite well with the value measured with this antenna. (See Appendix C.)

4.5 SUN-DRIFT CURVES

For antenna beam positions of $+16^{\circ}$ and $+31.2^{\circ}$ the antenna was pointed with the main beam looking directly at the sun by maximizing the output signal. Then, the output of the radiometer was recorded while the sun drifted through the antenna response curve, i.e., the antenna pattern. From this data the antenna half-power beamwidth was measured and the sun's brightness temperature calculated. It is possible to obtain the antenna pattern as well from the measurement.

Two sun-drift curves were made at $+31.2^{\circ}$, one using the standard gain horn as a reference load, the other using the cold reference load filled with liquid nitrogen. One drift curve was made at $+16^{\circ}$ using the cold reference load, this being done on a different day than the two measurements at $+31.2^{\circ}$. Plots of these responses are shown in the figures of Appendix D.

Table 4-2 shows the half-power beamwidths and sun temperatures obtained from these measurements, as well as the half-power beamwidths obtained from antenna patterns measured at the SGC antenna range at a single frequency. The accuracy of the measurements in either case is on the order of 0.1° thus reasonable correlation was established. The patterns measured on the antenna range were for the two principal planes of the antenna, while the sun-drift path was slightly skewed from the ϕ reference plane. This is discussed further in Appendix D, along with the sun temperature calculations. This measurement assumes that the antenna pattern is symmetrical, a condition which is closely approximated.

A further discussion of the sun-drift measurements can be found in Appendix D.

Table 4-2

MEASUREMENTS

Date	Time	Elevation Angle, Sun	Electrical Beam Position	Beamwidth from Sun-Drift Curve	Principal Plane Beamwidth from Antenna Range		Measured Sun Temp.
					θ	ϕ	
2-21-67	1222	44°	$+16^{\circ}$	2.91°	2.44°	2.98°	$7080^{\circ}K$
2-17-67	1445	34°	$+31.2^{\circ}$	3.02°	2.71°	2.98°	$7100^{\circ}K$
2-17-67	1533	23°	$+31.2^{\circ}$	3.04°	2.71°	2.98°	$7200^{\circ}K$

Section 5

CONCLUSIONS

Absolute measurements of the major characteristics of any antenna which is intended for radiometric applications rely upon the use of resistive sources at known temperatures; sources heated and regulated by resistive networks and control amplifiers, as well as sources maintained at cryogenic temperatures have been very useful and practical. These sources are necessary not only in providing comparison standards for the antenna brightness temperatures but also to accurately calibrate the radiometer receiver used in performing the measurements. The accuracy of these radiometric sources determines to a large degree the accuracy of the antenna parameter measurements. In addition, other factors contribute to the overall accuracy to be sure, among the most important being the antenna thermal temperature.

The results of these measurements on this particular antenna show that the calculated values of errors expected are in close agreement with those actually observed. For example, the average insertion loss at 0^{o} beam position was found to be $2.57 \pm .09$ dB which includes variations with temperature. At all other beam positions, the loss averages fell below this range of errors.

Some refinements in the beam efficiency measurement are evidently necessary; however, the measurements where the disk did not fill the main beam were performed on days when the winds were very gusty, not the best condition under which to perform this particular measurement. The average value of three beam efficiency measurements at 0^{o} beam position when performed under more ideal conditions was $87.5\% \pm 1.5\%$, which agrees quite favorably to a value of 88.9 percent obtained from a single frequency pattern integration. It is expected that the beam efficiencies measured radiometrically, i.e., broadband integration using the radiometer receiver as a measuring device, would be somewhat different than values obtained at a

single frequency. In most cases the radiometric measurement will give lower efficiency since the antenna is optimized at the center frequency but this was not true for a beam position of -16^{o}.

The antenna loss is appreciably higher than the design goal of 1.3 dB but the beam efficiency is quite close to the design goal of 92 percent. The antenna has proved to be electronically steerable and the radiometer was proved to have a sensitivity of less than $0.7^{o}K$ and capable of performing absolute measurements of better than $\pm 1^{o}K$. It must be further pointed out that this breadboard unit, including the radiometer receiver and electronically steerable array, operated over a range of temperature approximately equal to the specified values of $0^{o}C$ to $+ 50^{o}C$.

The sun temperature measurement proved to be quite interesting. Generally accepted values of the sun temperature at radio frequencies are approximately $6000^{o}K$ from the submillimeter band down to approximately 1 cm (30 GHz). At this point the temperature of the quiet sun varies up to a maximum value of 1 million ^{o}K at a wavelength of 5 meters. In the 1 to 2 cm band the temperature is generally believed to be from 6,000 to 10,000 ^{o}K and according to this measurement is around $7,100^{o}K$ at 1.5 cm.

Appendix A

BENCH CALIBRATION OF MICROWAVE RADIOMETER

A.1 INTRODUCTION

This radiometer is of the Dicke-type with an additional RF switch inserted between the Dicke switch and antenna (see Figure A-1). The purpose of the additional switch is to allow switching from the antenna port to a calibration port where a fixed known temperature load is placed. This allows measurement of the system gain in terms of radiometric temperature at regular intervals.

Calibrating this type of radiometer is relatively straightforward. The two external microwave inputs are labeled the antenna port and the calibration load port, respectively. These two ports, together with a third port terminated in a hot radiometric reference load, constitute the three inputs to the microwave switching network located between the signal antenna and the receiver. These ports are as labeled in Figure A-1.

In the discussions devoted to the radiometer calibration procedures the following assumptions are made:

a. The voltage reflection coefficients associated with the microwave switches (cal switch, S_1, and Dicke switch, S_2) are sufficiently small so that the mismatch insertion losses are negligible compared to the dissipative components of the forward direction insertion losses.

b. The impedance mismatches of the terminations on Ports 1, 2, 3, 4 and 5 are sufficiently low so that all power reflection coefficients are less than 10^{-3} (i.e., VSWR < 1.06).

c. The intrinsic isolation between two adjacent ports of the circulator switches is sufficiently high so that the observed isolation is determined solely by the power reflection coefficient of the third port.

d. The input circulator of the receiver has sufficiently high isolation so that the excess temperature of the receiver as seen at Port 5 is within $1^{\circ}K$ of the thermal ambient temperature of the receiver.

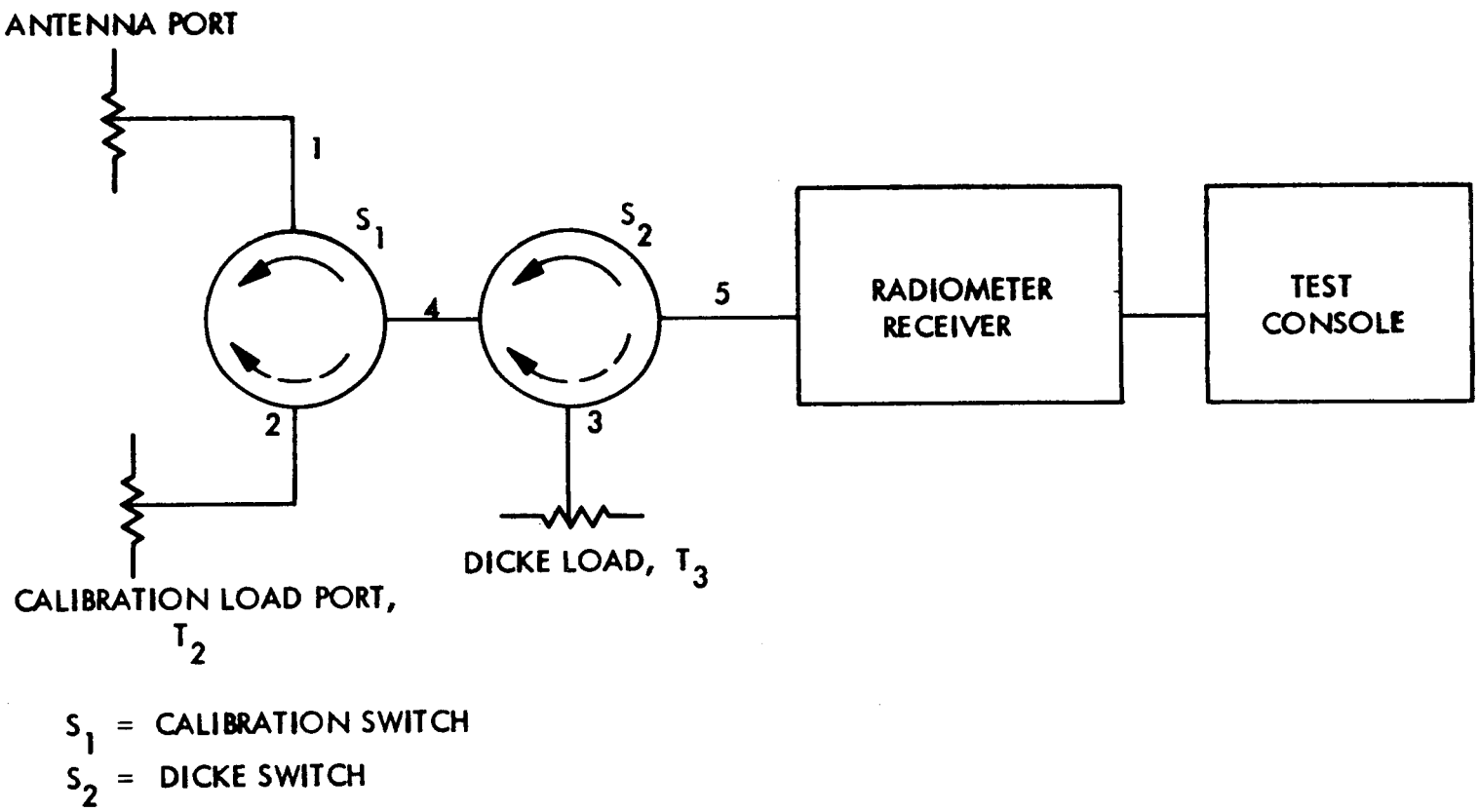

Figure A-1. Radiometer Switching Network

e. The isolation of the input circulator of the receiver is sufficiently high so that the receiver gain is totally independent of any impedance variations introduced by the switching network to the left of Port 5.

With these conditions satisfied (or nearly so) it is possible to relate the radiometric temperature of the switching network outputs at Port 5 to the radiometric temperatures of the terminations at Ports 1, 2 and 3, the insertion losses of the transmission paths, and the thermal temperatures of these losses.

The radiometric temperature outputs corresponding to the various combinations of the settings of the switches are (see list of definitions):

S_1	S_2	T_{in}
1 or 2	3	$T_{in} = \frac{T_3}{L_{35}} + \left(\frac{L_{35} - 1}{L_{35}}\right) T_{amb}$
1	4	$T_{in} = \frac{T_1}{L_{15}} + \left(\frac{L_{15} - 1}{L_{15}}\right) T_{amb}$
2	4	$T_{in} = \frac{T_2}{L_{25}} + \left(\frac{L_{25} - 1}{L_{25}}\right) T_{amb}$

List of definitions for terms in equations are as follows:

T_n radiometric temperature of the terminations at Ports $n = 1, 2$ and 3.

L_{n5} insertion loss from Ports $n = 1, 2$ and 3 and Port 5.

T_{amb} thermal ambient temperature of the transmission paths in the switching network

G_r radiometer gain coefficient, volts per degree Kelvin.

Since the Dicke switch is switching between Positions 3 and 4 at a periodic rate and the calibration switch is switched only at non-periodic intervals, the radiometer output voltages are

Position of S_1	Output Voltage
1	$V_{o1} = G_r \left[\frac{T_3}{L_{35}} + \left(\frac{L_{35} - 1}{L_{35}} \right) T_{amb} - \frac{T_1}{L_{15}} - \left(\frac{L_{15} - 1}{L_{15}} \right) T_{amb} \right]$
2	$V_{o2} = G_r \left[\frac{T_3}{L_{35}} + \left(\frac{L_{35} - 1}{L_{35}} \right) T_{amb} - \frac{T_2}{L_{25}} - \left(\frac{L_{25} - 1}{L_{25}} \right) T_{amb} \right]$

Terminations 2 and 3 are used as radiometric references to establish the overall system gain and, thus, provide an absolute scale which relates the radiometric temperature at Port 1.

Absolute measurements of gain and antenna temperatures may be accomplished in two ways. The first method requires that L_{15}, L_{25} and L_{35} be accurately known as well as their thermal temperature, T_{amb}. Then, by measuring the output voltage under the two switch positions of S_1, one can solve for T_1.

A somewhat simpler way to achieve the absolute gain is to make all the losses equal (i.e., $L_{15} = L_{25} = L_{35}$), which results in the following equations:

Position of S_1	Equation
1	$V_{o1} = G_r' (T_3 - T_1)$
2	$V_{o2} = G_r' (T_3 - T_2)$

The losses may be equalized by adding some dissipative loss to whichever transmission paths require it, taking the value of the path with the greatest loss as the final value of L. Over a 330°K antenna brightness temperature range the three losses must be equal to within 0.03 dB to cause an error of less than 1°K.

When the conditions of equal loss are established the gain constant is measured whenever the calibration switch is switched to the termination, T_2

$$G_r' = \frac{V_{o2}}{T_3 - T_2}$$

and, thus,

$$T_1 = T_3 - \frac{V_{o1}}{V_{o2}} (T_3 - T_2)$$

It is apparent from the above equations that, if the insertion losses in all three transmissions paths in the switching network are equalized and Ports 1, 2 and 3 are terminated in equal temperature loads, the radiometer zero is established. Also, the output is independent of the three termination temperatures; thus, a zero check can be performed for any termination temperatures.

The first stage of the radiometer calibration consists of establishing the radiometer zero setting and equalizing the switching network insertion losses. This equalization eliminates the dependence of the radiometer calibration on the ambient temperature of the switching network, provided the insertion losses are sufficiently constant within the required 0° to 50°C ambient temperature range. Even if the insertion losses vary slightly the temperature dependence is greatly reduced to a point where any corrections required using the switch (module) temperature monitor output should amount to less than 3°K over the full range of 0° to 50°C ambient.

A.2 STEPS IN BENCH CALIBRATION

A.2.1 RADIOMETRIC ZERO SETTING AND EQUALIZATION OF MICROWAVE SWITCHING NETWORK INSERTION LOSSES

A.2.1.1 RADIOMETRIC ZERO SET

The RF portion of the radiometer is brought to an ambient temperature of 35°C together with all three of the matched terminations. For this condition the radiometric temperature presented by the switch output

Port 5 to the receiver input is independent of the insertion loss associated with a particular selection of Ports 1, 2 and 3. Consequently, the radiometer output voltages corresponding to S_1 positions 1 and 2 should both be equal to zero. This procedure provides an output voltage reference corresponding to the radiometric zero point calibration. The individual steps of this measurement are described in the paragraphs following.

Place the radiometer in an oven stabilized to within $\pm 0.5^{\circ}C$ at $35^{\circ}C$. The hot reference load heater is disconnected and matched waveguide loads are placed on the two external waveguide ports normally occupied by the signal antenna and the cold reference.

Calibrated thermistors are placed on each of the two external loads and also on the aluminum block housing the two ferrite switches. These three thermistors, together with the monitor thermistor in the internal reference load, are continuously monitored to provide a record of the termination temperatures and the temperature of the ferrite switches.

Sufficient time must be allowed with the radiometer operating in the temperature controlled oven to insure that the switches and loads on temperatures become equalized and stabilized to within $\pm 0.2^{\circ}C$. In this condition the radiometer output voltage is measured at the output of the synchronous detector by means of an operational amplifier integrator housing a 10-second (6 dB per octave) integration time.

This will result in the peak-to-peak fluctuations of the radiometric output voltage originating from receiver thermal noise to correspond to approximately 0.4° peak-to-peak fluctuations in the radiometer input temperature. It is, thus, apparent that if the measurement is to be limited only to receiver thermal noise, then fluctuations in the thermometric temperature of the receiver source must be smaller, e.g., $\pm 0.2^{\circ}K$ occurring at a periodically large time compared to the integration time.

The output voltage is then recorded simultaneously with the four thermistor bridge output voltages and a timing marks with a calibrated six-channel chart recorder.

The radiometer output voltage is then observed under the following conditions:

a. With RF Switch S_1 set at the signal antenna Port 1

b. With the Switch S_2 set at the cold reference Port 2

c. With the 600 cps drive removed from the modulator RF Switch S_2.

NOTE: The radiometer output voltage (previously measured in the pick-up and ground-loop tests) with modulator Switch S_2 operating but with the receiver input disconnected from the switch output by means of a metal window across the guide connecting the Switch S_2 output to the receiver input isolator, gives the component of radiometer output voltage due to electromagnetic coupling between the Switch S_2 drive coil and the video amplifier.

The difference between the average of the voltages measured in Step a and Step b, and the output voltage measured in Step c, (above paragraph) gives the magnitude and sign of the radiometer output which is the summation of the voltages resulting from any slight thermal differences in the switches and terminations, synchronous variation of the reflection coefficients looking into Switch S_2 from the receiver direction, and electromagnetic pickup of the 600 cps by the video amplifier due to ground loops and electromagnetic coupling from the drive coil of the modulator Switch S_2. Since this ground loop and pickup voltage has been previously measured, the difference is the radiometer output component resulting from small temperature differences and synchronous modulation of the reflection coefficient presented to the receiver.

Although it is anticipated that this quantity will correspond to a temperature difference of less than $1^{o}K$ it is important to obtain quantitative verification.

The difference of the output voltage magnitudes obtained in Steps a and b is indicative of the degree to which the temperatures of the external port terminations differ from each other and any differences in their impedance match.

From a previous approximate calibration of the radiometer it is possible to relate these voltages to relative temperature differences. The voltages obtained in Steps a, b and c should each correspond to less than $1^{o}K$ temperature difference.

The average of Voltages a and b then correspond to zero radiometric temperature difference within the limits of the experimental ability to measure temperatures of the three sources and the switches.

With the radiometer zero point established the insertion loss equalization of the switching network can be initiated.

A.2.1.1.1 EQUALIZATION OF INSERTION LOSS FROM PORTS 1 AND 2 TO PORT 5

Place two $65^{o}C$ hot loads on Ports 1 and 2 with the reference hot load remaining at the $35^{o}C$ ambient temperature of the Switches S_1 and S_2. Then, observe the radiometer output voltage and observe with Switch S_1 set at Port 1 and then at Port 2. Then, interchange the loads on Ports 1 and 2, and again observe the output voltages with S_1 set at 1 and at 2. Designating the two sets of voltages as v_{a1}, v_{b1}, and v_{a2}, v_{b2}, respectively, the radiometer voltage output due to any radiometric temperature difference in the two sources is given by

$$ST = \frac{\left(v_a - v_b\right)_1 - \left(v_a - v_b\right)_2}{2g}$$

while the radiometer output voltage due to difference in the insertion losses L_{15} and L_{25} is proportional to

$$\Delta T = \frac{\left(v_a - v_b\right)_1 + \left(v_a - v_b\right)_2}{2g}$$

where g, the approximate radiometer gain coefficient, is expressed in terms of the average voltage output increase 'V' over the previously established radiometer zero output by the relation

$$g = \frac{V}{T_H - T_o} = \frac{V}{(65 - 35)^{\circ}K}$$

the difference between the two attenuations L_{15} and L_{25} is determined from the indicated radiometric temperature difference ΔT.

$$\Delta T = \left[\frac{T_H}{L_{15}} + \left(\frac{L_{15} - 1}{L_{15}}\right) T_o\right] - \left[\frac{T_H}{L_{be}} + \left(\frac{L_{25} - 1}{L_{25}}\right) T_o\right]$$

assuming

$$L_{15} = L_{25}(1 + \delta), \text{ and } (L_{15} - 1) \ll 1$$

$$T_o < T_h$$

The differential attenuation δ equals

$$\delta = \frac{\Delta T}{T_H - T_o}$$

attenuation is added to the lower attenuation input port until ΔT in the above equation is reduced to $0.2^{\circ}K$. Previous insertion loss measurements indicate approximately 0.08 dB corresponding to an initial value of ST = .02 and $\Delta T \approx 6^{\circ}K$.

A.2.1.1.2 EQUALIZATION OF INSERTION LOSS FROM PORT 3 to PORT 5

With Ports 1 and 2 giving the same radiometric indication, the heating element in the reference hot load on Port 3 is then activated, allowing at least one hour for the temperature to stabilize to the value $T_H = 65^{\circ}C$. The radiometer output is then observed with the Switch S_1 in either position 1 or 2. Now, all three ports are terminated in the same temperature to within the accuracy of the monitor thermistors in the three hot loads. If the insertion loss L_{35} equalled L_{15} and L_{25}, the radiometer output voltage would be equal to the previously determined radiometric zero value. The same procedure of interchanging hot loads is used to eliminate the effects of load temperature differences and attenuation is added to transmission path 35 until the output voltage equals the radiometric zero value with $\pm 0.2^{\circ}K$.

A.2.1.1.3 CHECK OF TEMPERATURE SENSITIVITY OF INSERTION LOSS EQUILIZATION

Maintaining the hot loads on the three ports at 65°C, the ambient temperature of the radiometer is then very slowly (over a period of four hours) reduced to 0°C and the output voltage change observed. If the load monitor thermistors readings remain unchanged then any change in the output voltage is a readiometric zero shift resulting either from a gain change in the receiver electronics or more likely from attenuation unbalance resulting from attenuation change with temperature in the ferrite Switches S_1 and S_2. The same observation should be made with a 50°C ambient temperature for the radiometer. Repeating these measurements should permit correlation of readiometric zero drift with ambient temperature and, thus, allow the derivation of a radiometric data correction factor for use with the switch monitor thermistor data output record; e.g., in the above measurements as the ambient is changing it should be possible to obtain a repeatable curve of radiometric zero shift as a function of the switch temperature monitoring thermistor.

A.3 RADIOMETER CALIBRATION WITH EXTERNAL RADIOMETRIC TEMPERATURE REFERENCES

The radiometric zero setting and the insertion loss equalization of the switching network is completed. Calibration of the radiometer output voltage versus varying antenna port temperature for several different values of fixed temperature terminations on Port 1 can be performed. Interchanging the radiometric sources with the various fixed temperature terminations on the antenna Port 1 and varying the cold reference Port 2 termination should produce the same radiometric output. Repeating these procedures for several different ambient temperatures between 0°C and 50°C and employing, if necessary, any ambient temperature dependent correction factors previously determined in Section A.2.1.1.3, should establish the absolute accuracy to which the radiometric temperature of the antenna port can be ascertained from the radiometric output voltage and knowledge of the hot and cold reference ports radiometric temperatures and the switching network ambient temperature.

When these steps in the basic calibration procedure have been completed, an accurate temperature calibration curve may be obtained using the cold load bench test set described in Appendix B. Such a curve was obtained using this bench test set and is shown in Figure A-2 for both liquid nitrogen and liquid helium. Note that the gain of the system in counts per degree Kelvin is the reciprical of the slope of the calibration curve. The gain under these two conditions is different due to the nature of the radiometer AGC, which is discussed in the original proposal to NASA Goddard for the entire radiometer (SGC P-6308). The value of the offset is roughly 2 counts or $1^{o}K$.

The radiometer sensitivity was measured and found to be consistently better than $0.66^{o}K$ rms, which is somewhat better than the required specification of $0.70^{o}K$.

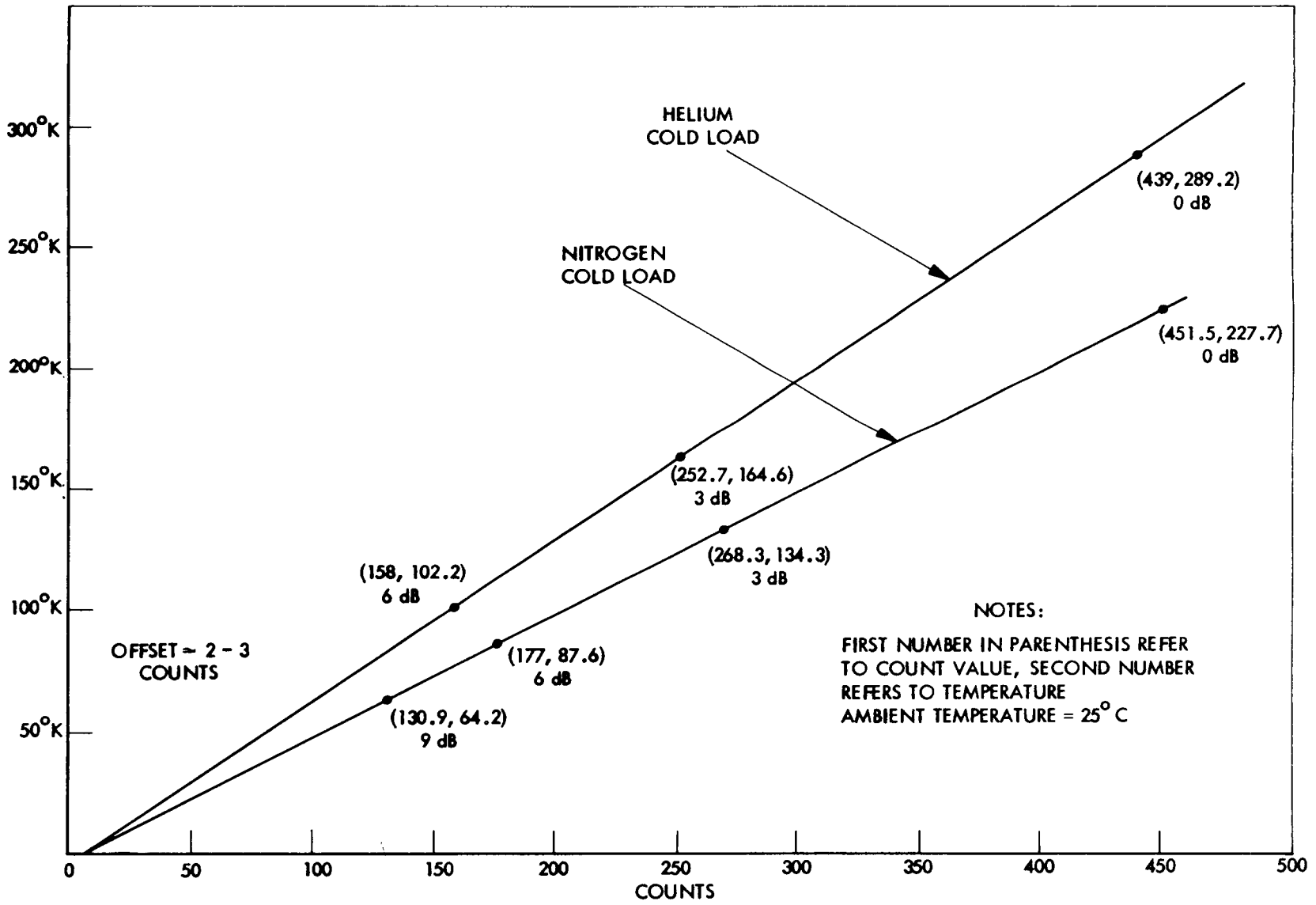

Figure A-2. Typical Calibration Curves of Radiometers Using Bench Test Set

Appendix B

COLD LOAD TEST SET

B.1 INTRODUCTION

The purpose of the cold load bench test set is to provide an accurate temperature calibration of the radiometer response as a function of antenna brightness temperature. Secondary results of such a calibration are to provide a linearity check and to correlate previous measurements of the amount of offset produced when the radiometer antenna temperature is equal to the radiometer Dicke temperature; i.e., the temperature of the hot load located inside the radiometer module. This is done by extrapolation of the calibration curve. The value of offset obtained may then be compared to values obtained in previous bench calibrations. The exact testing procedure used will be described below. Once the radiometer response is established, the radiometer may then be used to measure the antenna parameters and to perform absolute radiometric measurements.

B.2 DESCRIPTION OF THE COLD LOAD TEST SET

Briefly, the cold load test set is constructed as follows: two matched terminations are heat-sunk to a Texas Instruments' cryoflask. The vacuum seal of this flask is maintained by the insertion of two matched mica windows into the flange which is sealed to the side of the cryoflask. Two lengths of waveguide join this flange to another flange which is the output port of the bench test set. One waveguide arm contains a calibrated precision attenuator, the other contains only various sections of waveguide. The attenuator arm connects to the radiometer antenna port, the other goes to the radiometer calibrate port. The cryoflask may be filled with cryogenic liquids such as nitrogen or helium to bring the loads down to the liquid temperatures. A block diagram of the test set is shown in Figure B-1.

Since the resultant radiometric temperature of a load at a designated temperature is a function of various power transmission parameters

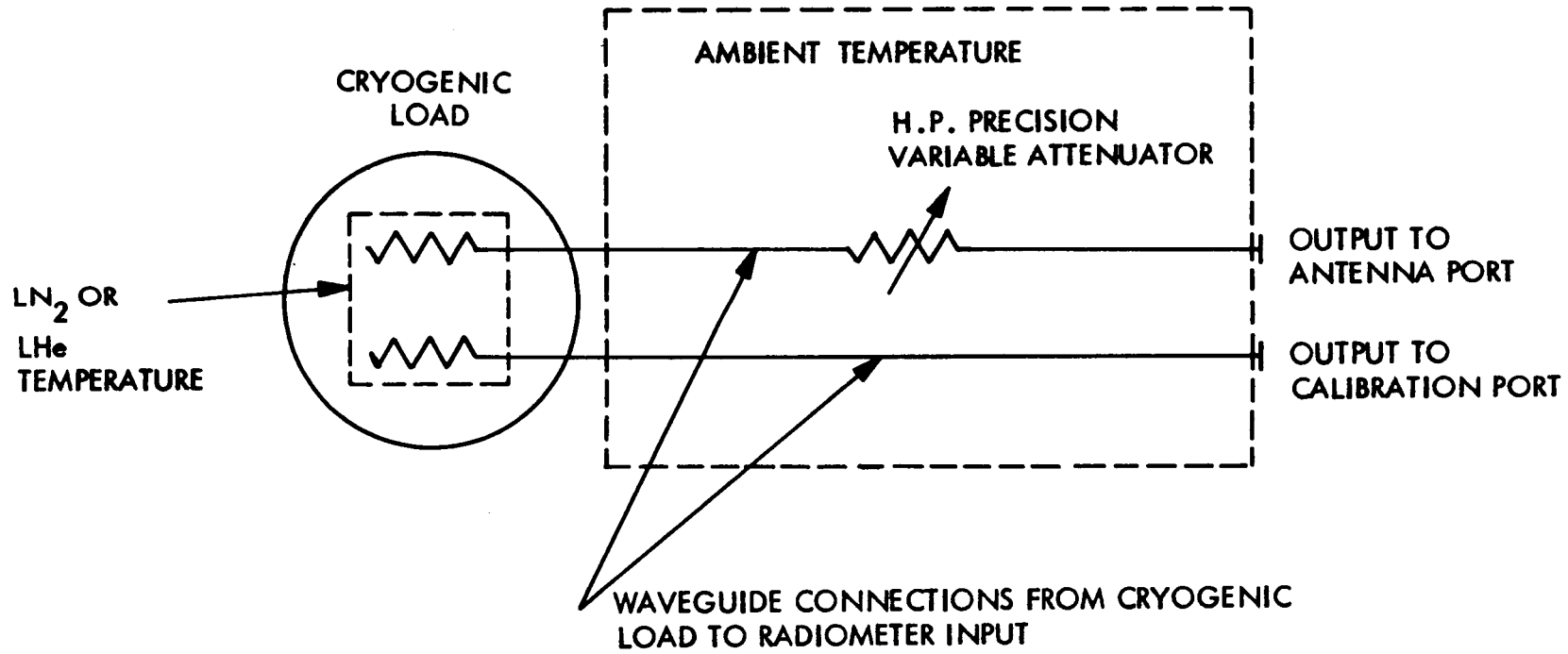

Figure B-1. Block Diagram of The Cold Load Bench Test Set

existing between the observation port and the load, the numerous losses present (both dissipative and reflective) must be known to a considerable degree of accuracy. With this end in view, the total insertion losses and standing wave ratios of both arms were measured. The same measurements were made with the individual arm components as well as with the mica window and the plated waveguide inside the cryoflask itself.

The Hewlett-Packard precision attenuator used in the antenna arm was measured for residual insertion loss at four different settings: 0, 3, 6, and 9 decibels. Since this residual loss is either constant or increases slightly (and in a linear fashion with attenuation), interpolation of the measured losses to obtain losses for other attenuator settings poses no problem. The drift of the attenuator with a $50^{\circ}C$ temperature range was also measured and found to be negligible (approximately 0.005 dB). Incidentally, the 0-decibel residual loss of 0.46 decibels causes the apparent temperature of the attenuator arm to be always greater than that of the calibration arm.

To know the radiometric brightness temperature of the bench test set to within $1/2^{\circ}K$ or less, it was necessary to make all insertion loss measurements on the SGC insertion loss test set, which is modeled after the test set proposed by C. T. Stelzried and S. M. Petty of JPL in the IEEE Transactions on Microwave Theory and Techniques. The following is a quotation of the article's summary:

> "A simple, accurate test set has been devised for measuring insertion losses at microwave frequencies. It is composed almost entirely of commercially available equipment and components. The short-term jitter is about 0.0004 dB peak-to-peak, and long-term drift is typically 0.0015 dB per hour. Accuracy of the measurements depends upon the value of the insertion loss to be measured and is better than ± 0.001 to ± 3 percent for insertion losses in the 0 to 25 dB range. These accuracies include the non-repeatability of connecting and disconnecting the waveguide flanges used in the system."

The accuracy of the SGC test set is believed to be better than 0.003 dB for small losses.

VSWR measurements of the waveguide sections, attenuator, and window were made on a Hewlett-Packard slotted line. Both the VSWR and the phase of the reflection coefficient were measured for each item. Attenuation

measurements for each piece of waveguide and the attenuator were made a number of times on the insertion loss test set to minimize errors due to drifts in the test set. Averages were taken to determine the various values for loss.

B.2 OUTPUT TEMPERATURES OF THE COLD LOAD TEST SET

Computations of apparent brightness temperature were carried out using the model in Figure B-2 for the test set.

a. The load is assumed to be at the boiling point of the cryogenic liquid in the flask. This is thermometric temperature, t_L, and it gives the matched termination a radiometric brightness temperature, T_L.

b. Between the termination and the mica window is a length of stainless steel waveguide with a constant loss per unit length and a linear temperature distribution between the boiling point temperature of the cryogenic liquid and the prevailing ambient temperature. These temperatures are t_L and t_A, respectively.

c. The equivalent radiometric temperature seen at the output of the guide is given by $T_{eq} = T_L + (t_A - t_L)(1 - 1/L_1)/\mathcal{L}$ where $\mathcal{L} = 0.23026\ L_1$ (dB). Note that T_L is numerically equal to t_L.

d. The temperature seen just past the mica window due to reflective losses only is given by:

$$T' = \frac{(1 - |\Gamma_1|^2)(1 - |\Gamma_2|^2)}{(|1 - \Gamma_2 \Gamma_3|)^2} \quad T_{eq}$$

This is the equation representing power delivered to a mismatch load by a mismatch generator. Note that the phases of Γ_1 and Γ_2 are required in the denominator.

e. When the dissipative loss of the window is taken into account, the resulting radiometric temperature is given by: $T_1 = T'/L_2 + t_A(1 - 1/L_2)$.

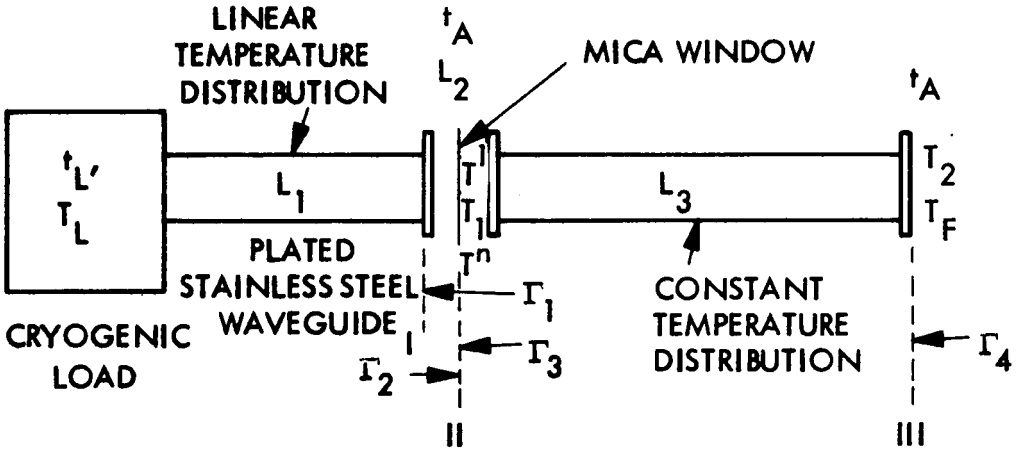

Figure B-2. Model for Cold Load Test Set Calibration

f. Reflections between the mica window and the external waveguide cause more loss. The equation for this reflective loss is:

$$T'' = \frac{(1 - |\Gamma_2|^2)(1 - |\Gamma_3|^2)}{(|1 - \Gamma_2 \Gamma_3|)^2} \; T_1$$

g. The dissipative loss of the external waveguide arms is taken into account in the same manner as the window loss, since the waveguide is at the constant temperature t_A. This gives the output temperature of the bench test set as: $T_F = T''/L_3 + t_A (1 - 1/L_3)$.

h. The output temperature, T_F, of the test set is <u>not</u> the same as that seen by the radiometer because the set presents a certain VSWR to the radiometer and, hence, reflects a certain portion of the radiometer's own brightness temperature back into the radiometer itself. This can be corrected for by adding the term $|\Gamma_4|^2 t_A$ to the output temperature, T_F. This is the apparent brightness temperature seen by the radiometer.

B.4 ERROR ANALYSIS

For losses less than 0.5 dB, the equivalent temperature at the output of the stainless steel waveguide may be expressed accurately as:

$$T_{eq} = T_L + .115 (t_A - t_L) L$$

The maximum uncertainty in T_{eq} is then given by:

$$\Delta T_{eq} = |\Delta T_L| + .115 (t_A - t_L) |\Delta L| + .115 L |\Delta(t_A - t_L)|$$

The loss of this section of waveguide is approximately 0.06 dB and is known to well within $\pm$ 0.003 dB. For $t_A - t_L \simeq \pm 210^{\circ}K$ and $\Delta(t_A - t_L) \simeq \pm 0.2^{\circ}K$ the uncertainty in ΔT_{eq} is

$$\Delta T_{eq} = |\Delta T_L| + .072 + .0014 = (|\Delta T_L) + .0734)$$

The boiling point of the cryogenic used is known very well (see Table B-1) for various pressures. The uncertainty in the actual temperature of the resistive portion of the load is felt to be less than $0.1^{o}K$ resulting in an uncertainty in ΔT_{eq} of less than $.175^{o}K$.

For the reflection loss equations, we have:

$$\Delta T' = \Delta T_{eq} \left[\text{mismatch factor}\right] + \Delta(\text{mismatch factor terms})\, T_{eq}$$

Since Γ's are always $\ll 1$, the mismatch factor is usually .999X, where $1 \leq X \leq 9$ and X is known to ± 2 from measurement. Hence, $\Delta(\text{mismatch factor terms}) \leq 10^{-3}$ and the term of significance is still ΔT_{eq}.

Further analysis indicates that the significant error still lies in the uncertainty in the load temperature, T_L, which determines to a great degree the uncertainty in T_{eq}. All other terms combined add a negligible amount to the uncertainty in T_F, because of the accuracy of the insertion loss measurements and the negligible effect of the small reflections. The accuracy of T_F is then equal to the accuracy in knowing T_{eq}. Since $\Delta T_{eq} = .175^{o}K$, one can perform an absolute calibration of this radiometer to within $\pm 1^{o}K$ with a high degree of probability.

Table B-1

CRYOGENIC BOILING POINTS

Pressure	Temperature	
Mm. Hg.	Helium	Nitrogen
1	1.3°K	47.0°K
10	1.8°K	54.0°K
40	2.2°K	59.1°K
100	2.6°K	63.4°K
400	3.9°K	72.2°K
760	4.2°K	77.3°K

Boiling Points of Liquid Helium and Nitrogen

The expression in the denominator of the third equation indicates the necessity of making phase measurements. However, a sample calculation shows that errors made by assuming the denominator is equal to 1.0000 are negligible; that is, they are about equal to one part in 10^4.

The relevant equations were solved for sixty discrete values of ambient temperature and for four attenuator settings, using an IBM System-360 computer. The resulting printouts (see Tables B-2 and B-3) give the apparent radiometric temperatures at the antenna and calibration ports as a function of both ambient temperature and attenuator setting for both liquid nitrogen and liquid helium.

To use the test set as a calibration device, one must first note the ambient temperature and pressure. The pressure determines the boiling point of the cryogenic liquid used in the flask, and the temperature determines the apparent output temperature as read from the computer tables. Differences in boiling points may be added directly to the computed results with negligible error.

After connecting the test set to the radiometer through waveguide sections whose loss is precisely known, one actuates the radiometer and gathers several frames of digital output. The average of 100 antenna temperature counts is computed, as is the average of all the calibration port counts. This is done for a number of attenuator settings on the test set. If the calibration count is found to drift, the antenna average for a given run may be corrected by multiplying it by the ratio of the first calibration count to the calibration count for the run of interest.

It is now possible to plot antenna counts versus radiometric temperature. The resulting graph should be a straight line, but only if the apparent cold load temperatures are first subtracted from 339.0 degrees Kelvin, the temperature of the Dicke load inside the radiometer. It thus becomes apparent that as the radiometric temperature increases, the difference between it and the Dicke temperature becomes smaller and the output count diminishes. The intercept on the graph where this temperature equals zero gives a residual count which ideally should also equal zero but which, in fact, is on the order of this counts, or about 1 degree Kelvin, a value which agrees with the offset obtained in the measurements described in Appendix A.

Table B-2

COLD LOAD BENCH TEST SET OUTPUTS FOR
VARIOUS ATTENUATOR SETTINGS,
LIQUID NITROGEN

TLOAD OF NITROGEN = 77.3

TR	TRAD				CAL
	0	3	6	9	
261	108.07	184.65	222.85	242.06	95.07
262	108.24	185.23	223.64	242.96	95.17
263	108.41	185.82	224.44	243.86	95.26
264	108.58	186.40	225.23	244.76	95.36
265	108.74	186.99	226.02	245.65	95.46
266	108.91	187.57	226.81	246.55	95.56
267	109.08	188.16	227.61	247.45	95.65
268	109.25	188.74	228.40	248.34	95.75
269	109.42	189.33	229.19	249.24	95.85
270	109.58	189.91	229.98	250.14	95.95
271	109.75	190.50	230.78	251.03	96.04
272	109.92	191.08	231.57	251.93	96.14
273	110.09	191.66	232.36	252.83	96.24
274	110.26	192.25	233.15	253.72	96.33
275	110.42	192.83	233.95	254.62	96.43
276	110.59	193.42	234.74	255.52	96.53
277	110.76	194.00	235.53	256.41	96.63
278	110.93	194.59	236.32	257.31	96.72
279	111.10	195.17	237.12	258.21	96.82
280	111.26	195.76	237.91	259.11	96.92
281	111.43	196.34	238.70	260.00	97.02
282	111.60	196.93	239.49	260.90	97.11
283	111.77	197.51	240.29	261.80	97.21
284	111.94	198.10	241.08	262.69	97.31
285	112.10	198.68	241.87	263.59	97.41
286	112.27	199.26	242.66	264.49	97.50
287	112.44	199.85	243.45	265.38	97.60
288	112.61	200.43	244.25	266.28	97.70
289	112.78	201.02	245.04	267.18	97.79
290	112.94	201.60	245.83	268.07	97.89

Table B-2 (Continued)

COLD LOAD BENCH TEST SET OUTPUTS FOR
VARIOUS ATTENUATOR SETTINGS,
LIQUID NITROGEN

TLOAD OF NITROGEN = 77.3

TR	TRAD 0	3	6	9	CAL
291	113.11	202.19	246.62	268.97	97.99
292	113.28	202.77	247.42	269.87	98.09
293	113.45	203.36	248.21	270.77	98.18
294	113.62	203.94	249.00	271.66	98.28
295	113.78	204.53	249.79	272.56	98.38
296	113.95	205.11	250.59	273.46	98.48
297	114.12	205.69	251.38	274.35	98.57
298	114.29	206.28	252.17	275.25	98.67
299	114.46	206.86	252.96	276.15	98.77
300	114.62	207.45	253.76	277.04	98.87
301	114.79	208.03	254.55	277.94	98.96
302	114.96	208.62	255.34	278.84	99.06
303	115.13	209.20	256.13	279.73	99.16
304	115.30	209.79	256.93	280.63	99.25
305	115.46	210.37	257.72	281.53	99.35
306	115.63	210.96	258.51	282.43	99.45
307	115.80	211.54	259.30	283.32	99.55
308	115.97	212.13	260.09	284.22	99.64
309	116.14	212.71	260.89	285.12	99.74
310	116.30	213.29	261.68	286.01	99.84
311	116.47	213.88	262.47	286.91	99.94
312	116.64	214.46	263.26	287.81	100.03
313	116.81	215.05	264.06	288.70	100.13
314	116.98	215.63	264.85	289.60	100.23
315	117.15	216.22	265.64	290.50	100.33
316	117.31	216.80	266.43	291.39	100.42
317	117.48	217.39	267.23	292.29	100.52
318	117.65	217.97	268.02	293.19	100.62
319	117.82	218.56	268.81	294.08	100.71
320	117.99	219.14	269.60	294.98	100.81

Table B-3

COLD LOAD BENCH TEST SET OUTPUTS FOR
VARIOUS ATTENUATOR SETTINGS,
LIQUID HELIUM

TLOAD OF HELIUM = 4.2

TR	0	3	6	9	CAL
261	47.34	154.32	207.69	234.53	29.19
262	47.51	154.90	208.48	235.42	29.29
263	47.68	155.49	209.27	236.32	29.38
264	47.85	156.07	210.06	237.22	29.48
265	48.02	156.66	210.86	238.11	29.58
266	48.18	157.24	211.65	239.01	29.68
267	48.35	157.83	212.44	239.91	29.77
268	48.52	158.41	213.23	240.80	29.87
269	48.69	159.00	214.03	241.70	29.97
270	48.86	159.58	214.82	242.60	30.07
271	49.02	160.17	215.61	243.49	30.16
272	49.19	160.75	216.40	244.39	30.26
273	49.36	161.33	217.20	245.29	30.36
274	49.53	161.92	217.99	246.19	30.46
275	49.70	162.50	218.78	247.08	30.55
276	49.86	163.09	219.57	247.98	30.65
277	50.03	163.67	220.37	248.88	30.75
278	50.20	164.26	221.16	249.77	30.84
279	50.37	164.84	221.95	250.67	30.94
280	50.54	165.43	222.74	251.57	31.04
281	50.70	166.01	223.54	252.46	31.14
282	50.87	166.60	224.33	253.36	31.23
283	51.04	167.18	225.12	254.26	31.33
284	51.21	167.76	225.91	255.15	31.43
285	51.38	168.35	226.70	256.05	31.53
286	51.54	168.93	227.50	256.95	31.62
287	51.71	169.52	228.29	257.84	31.72
288	51.88	170.10	229.08	258.74	31.82
289	52.05	170.69	229.87	259.64	31.92
290	52.22	171.27	230.67	260.54	32.01

Table B-3 (Continued)

COLD LOAD BENCH TEST SET OUTPUTS FOR
VARIOUS ATTENUATOR SETTINGS,
LIQUID HELIUM

TLOAD OF HELIUM = 4.2

TR	TRAD 0	TRAD 3	TRAD 6	TRAD 9	CAL
291	52.38	171.86	231.46	261.43	32.11
292	52.55	172.44	232.25	262.33	32.21
293	52.72	173.03	233.04	263.23	32.30
294	52.89	173.61	233.84	264.12	32.40
295	53.06	174.20	234.63	265.02	32.50
296	53.22	174.78	235.42	265.92	32.60
297	53.39	175.36	236.21	266.81	32.69
298	53.56	175.95	237.01	267.71	32.79
299	53.73	176.53	237.80	268.61	32.89
300	53.90	177.12	238.59	269.50	32.99
301	54.06	177.70	239.38	270.40	33.08
302	54.23	178.29	240.18	271.30	33.18
303	54.40	178.87	240.97	272.20	33.28
304	54.57	179.46	241.76	273.09	33.38
305	54.74	180.04	242.55	273.99	33.47
306	54.90	180.63	243.34	274.89	33.57
307	55.07	181.21	244.14	275.78	33.67
308	55.24	181.79	244.93	276.68	33.76
309	55.41	182.38	245.72	277.58	33.86
310	55.58	182.96	246.51	278.47	33.96
311	55.74	183.55	247.31	279.37	34.06
312	55.91	184.13	248.10	280.27	34.15
313	56.08	184.72	248.89	281.16	34.25
314	56.25	185.30	249.68	282.06	34.35
315	56.42	185.89	250.48	282.96	34.45
316	56.59	186.47	251.27	283.85	34.54
317	56.75	187.06	252.06	284.75	34.64
318	56.92	187.64	252.85	285.65	34.74
319	57.09	188.23	253.65	286.55	34.84
320	57.26	188.81	254.44	287.44	34.93

Appendix B

REFERENCES FOR COLD LOAD TEST SET

1. A. J. Estin, C. L. Trembath, J. S. Wells, and W. C. Daywitt, "Absolute Measurement of Temperatures of Microwave Noise Sources," IRE Trans. on Inst. and Meas., pp. 209-213, Sept. 1960.

2. J. S. Wells, W. C. Daywitt, and C. K. S. Miller, "Measurement of Effective Temperatures of Microwave Noise Sources," IRE Trans. on Inst. and Meas., pp. 17-28, March 1964.

3. C. T. Stelzreid, "Temperature Calibration of Microwave Thermal Noise Sources," IEEE Trans. on Microwave Tehory and Techniques, pp. 128-130, Jan. 1965.

4. C. T. Stelzreid, "A Liquid Helium-Cooled Coaxial Termination," Proc. of IRE, p. 1224, July 1961.

5. R. C. Clauss, W. Higa, C. Stelzreid, and E. Wiebe, "Total System Noise Temperature: 15°K, "IEEE Trans. on Microwave Theory and Techniques, pp. 619-620, Nov. 1964.

6. C. T. Stelzreid, "Temperature Calibration of Microwave Terminations," JPL Space Programs Summary No. 37-26, Vol. IV, pp. 189-194.

7. C. T. Stelzreid and S. M. Petty, "Microwave Insertion Loss Test Set," IEEE Trans. on Microwave Theory and Techniques, pp. 475-477, July 1964.

8. R. C. Menon, N. P. Albaugh, and J. W. Dozier, "Cooled Loads as Calibration Noise Standards for the mm-Wavelength Range," Proc. of IEEE, pp. 1501-1503, Oct. 1966.

9. R. W. Beatty, "Mismatch Errors in the Measurement of Ultrahigh-Frequency and Microwave Variable Attenuators, Journal of Research of the National Bureau of Standards, pp. 7-9, Vol. 52, No. 6, June 1964.

10. R. W. Beatty, "Insertion Loss Concepts," Proc. of IEEE, pp. 663-671, Vol. 52, No. 6, June 1964.

REFERENCES FOR COLD LOAD TEST SET

11. J. E. Sees, "Fundamentals in Noise Source Calibrations at Microwave Frequencies," Naval Research Lab., Wash., D.C., Rept. No. 5051, 1958.

12. A. E. Siegman, "Thermal Noise in Microwave Systems," Part 1, Microwave Journal, pp. 81-90, March 1961.

13. D. Schuster, C. T. Stelzreid, and G. S. Levy, "The Determination of Noise Temperatures of Large Paraboloidal Antennas," IRE Trans. on Antennas and Propagation, pp. 286-291, May 1962.

Appendix C

ZENITH SKY TEMPERATURE

In this section the effective radiometric temperature of the sky in the zenith direction will be calculated for the 19.35 GHz region. Contributions to the zenith temperature, Tz, consist of three sources of radiation; that from the cosmic background, Tb; that from the radiation due to the oxygen in the atmosphere, T_{O_2}; and that from radiation due to the water vapor in the atmosphere, T_{H_2O}.

The zenith temperature, Tz, is given by:

$$Tz = \frac{Tb}{L} + T_{O_2} + T_{H_2O}$$

where L is the total zenith loss due to the O_2 and H_2O attenuation.

The cosmic black body radiation has only recently been discovered.[1][2][3] It appears to be isotropic, unpolarized and constant with regard to seasonal variations. In addition, from the limited number of observations made and from theoretical considerations, it appears to be independent of frequency. A measured value for this radiation at a frequency of 4080 MHz by BTL[1], using a low-noise hog-horn antenna, is $3.5^{\circ} \pm 1^{\circ}K$. Other values measured for Tb have ranged from $2\text{-}4^{\circ}K$. Since this measurement is a difficult one to perform, the value for Tb is still not accurately known. However, for the purpose of these measurements a value of $3.5^{\circ} \pm 1^{\circ}K$ will be used.

The absorption of oxygen and water vapor gases at microwave frequencies has been studied theoretically by Van Vleck[4], and the resultant radiant temperatures due to oxygen and water vapor have been calculated by Hogg[5], based on a standard model of the atmosphere shown in Figure C-1.

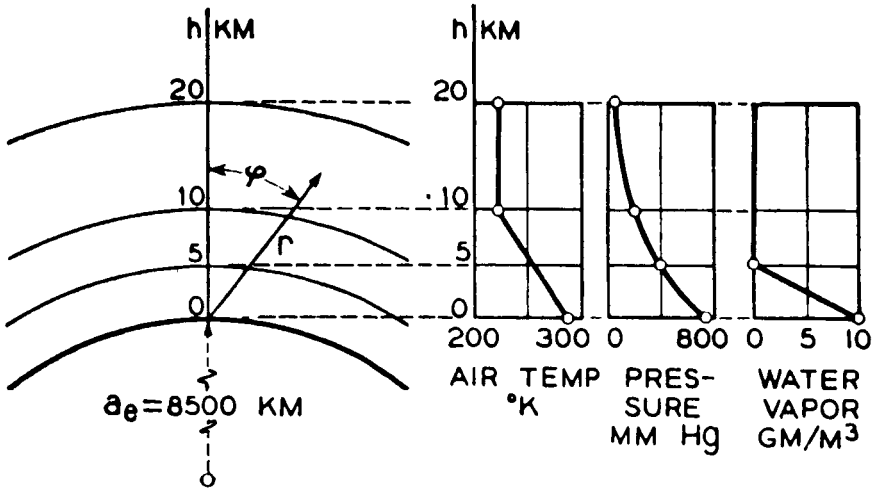

Figure C-1. Model of The Earth Assumed in Calculations

Attenuation due to oxygen is the result of resonances of the oxygen molecules at 60 GHz. Due to pressure broadening, the lines blend together to give a width of approximately 0.5 to 1 GHz.

A curve of temperature versus frequency for various zenith angles is shown in Figure C-2.[5] This is based on a standard atmosphere with a sea level pressure of 760 mm and a temperature of 290°K. At 19.35 GHz, we are well out on the skirt of the absorption curve and obtain a temperature of 3.4°K. Since the measurements were taken at a 7200-foot elevation, the absolute barometric pressure range was 588 to 5.94 mm/Hg. Thus, the radiated temperature would be reduced by approximately the ratio of the barometric pressures to a value of 2.64°K. The ambient temperature at 7200 feet ranged from 270°K to 288°K. For low values of attenuation the radiometric temperature is approximately a linear function of ambient temperature range and will be 2.46°K to 2.62°K. For the purpose of these measurements, an average value of 2.5°K will be used.

The atmospheric absorption due to the water vapor results from a resonance line at 22.5 GHz. Figure C-3 shows the radiometric temperature versus frequency for various zenith angles due to the presence of water vapor.[5] This is based on a water vapor content of 10 g/m^3 at sea level, linearly decreasing to 0 g/m^3 at an altitude of 5 Km. At a frequency of 19.35 GHz, the temperature is a rapid function of frequency since it is close to the resonance frequency, 22.5 GHz making it more difficult to obtain an accurate value of T_{H_2O}.

From Figure C-3, a value of $T_{H_2O} = 11.6°K$ is obtained for the zenith at 19.35 GHz. For low attenuation values such as we have here, T_{H_2O} will be approximately a linear function of the absolute humidity. The absolute humidity, ρ, is expressed in grams/m^3 and was calculated for each data run from the recorded air temperature and the relative humidity. The relative humidity was frequently low (0 - 15 percent) where it is difficult to measure accurately. Fortunately, however, the radiometric temperature contribution is small for low moisture content. Also, the sky was completely

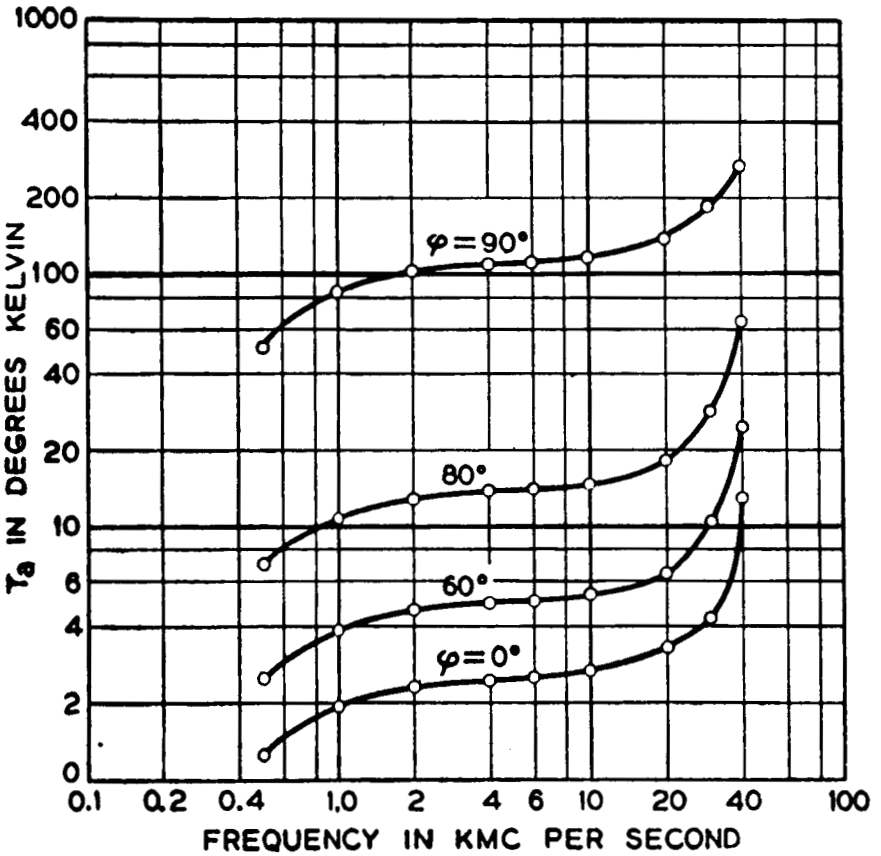

Figure C-2. Zenith Temperature Contribution from Oxygen

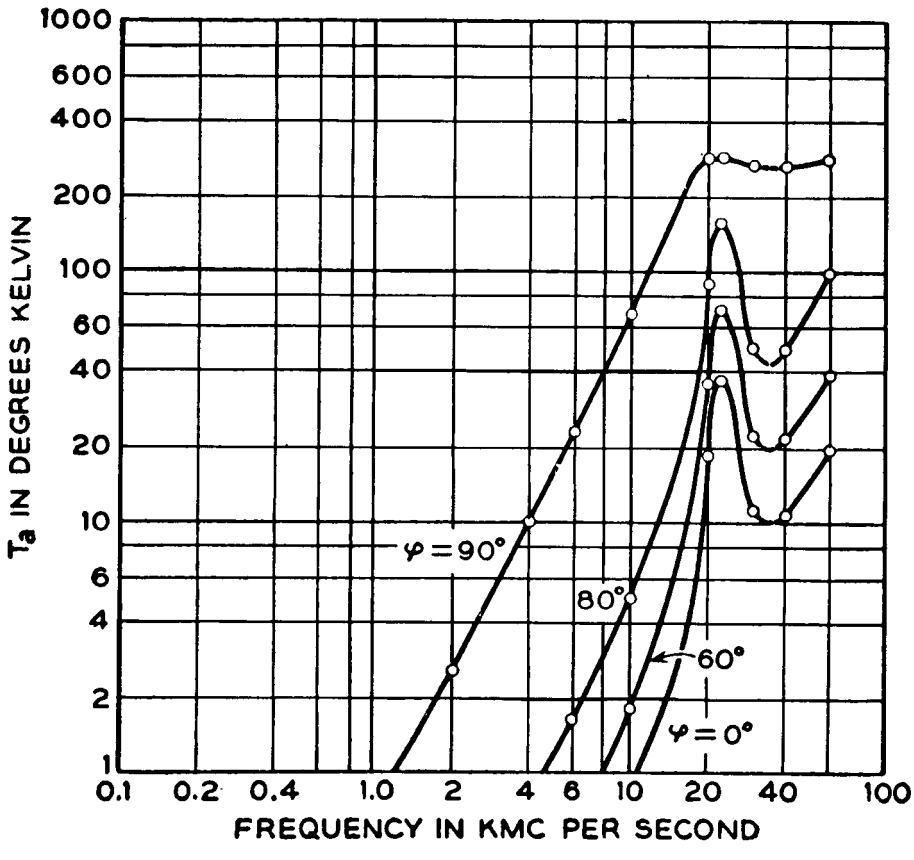

Figure C-3. Zenith Temperature Contribution from Water Vapor

clear for most runs with the exception of a few runs having high thin cirrus clouds below a 60^{o} zenith angle. Being at 7200 feet, the site was also above the temperature inversion layer which frequently occurs at lower altitudes in the Los Angeles basin, making the standard atmosphere curves of Figure C-1 applicable.

The following table lists the radiometric temperature received from the zenith as a result of water vapor attenuation alone as a function of absolute humidity for the extremes of ambient temperature, t_A, of $-3^{o}C$ and $17^{o}C$.

Table C-1

ATMOSPHERIC ZENITH TEMPERATURES

(Absolute Humidity)	T_{H_2O} (for $t_A = -3^{o}C$)	T_{H_2O} (for $t_A = 17^{o}C$)
0 gm/m^3	$0^{o}K$	$0^{o}K$
0.5	0.6	$0.6^{o}K$
1	1.1	$1.2^{o}K$
2	2.2	$2.4^{o}K$
3	3.3	$3.6^{o}K$
4	4.5	$4.8^{o}K$
5	5.6	$6^{o}K$
10	11.1	$12^{o}K$

The absolute humidity ranged from 0 to 3 gm/m^3 for all runs. Combining T_{O_2} and T_{H_2O} for $\rho = 3\ gm/m^3$, we get a zenith temperature due to the atmosphere of $4.9^{o}K$. This is equivalent to a total attenuation of 0.98 which attenuates the galactic background temperature by a small amount from $3.5^{o}K$ to $3.4^{o}K$.

Table C-2 summarizes the zenith sky temperatures.

Table C-2

ZENITH TEMPERATURE

Absolute Humidity	Cosmic Background Tb	Oxygen T_{O_2}	Water Vapor T_{H_2O}	Total Tz
0 gm/m^3	3.5°K	2.5°K	0°K	6.0°K
0.5	3.5	2.5	0.6	6.6
1	3.5	2.5	1.1	7.1
2	3.5	2.5	2.3	8.3
3	3.4	2.5	3.4	9.3
4	3.3	2.5	4.6	10.4
5	3.3	2.5	11.6	17.2

Since the absolute humidity was < 3 g/m^3 during the measurements the zenith temperature range was 6-10°K during the runs. While the error in absolute value of the zenith temperature is probably ± 2°K the relative values are probably accurate to ± 0.5°K for different runs. Since the zenith temperature is low the effect on the accuracy of the antenna measurement is small, as discussed in the previous sections. Additional references on atmospheric radiation are [6] and [7] which include the effects of clouds and precipitation.

REFERENCES

1. Penzias, A. A., and Wilson, R. W., 1965, Ap. J, Vol. 142, (419)

2. Dicke, R. H., Peebles, P. J. E., Roll, P. G., and Wilkinson, D. T., 1965, Ap. J, VI42 (414)

3. Thaddeus, P., Inst. for Space Studies, NASA, Priv. Communications.

4. Van Vleck, J. H., Phys. Rev., (1947) Vol 71, (413)

5. Hogg, D. C., J. A. P., 1959 Vol 30 (1417)

6. Hogg, D. C., and Semplak, R. A., B. S. T. J., Sept. p 961, (1331)

7. Orhaug, T., National Radio Astronomy Observatory, Greenbank, Vol. I, No. 14, Oct. 1962

Appendix D

SUN DRIFT CURVE

Since the sun is a strong source of thermal radiation at microwave frequencies and is relatively small in angular size it can be used as a source for calibrating the antenna and radiometer. The temperature of the sun is uniform across the disk and is equal to 6000°K or greater at 19 GHz. Its optical angular diameter is 32.4 minutes of arc. At 19 GHz the radio diameter and the optical diameter are almost equal.

By taking a cut of the sun with the antenna, the antenna pattern can be obtained. This is accomplished by positioning the beam to maximize the signal received from the sun. Then the mount is left stationary and the sun is allowed to drift through the antenna pattern. Because the sun moves through the sky at a constant 15° of arc per hour in right ascension or hour angle with a small change in declination ($\sim$0.1°/day), time can be converted into angular movement in degrees. Since the sun travels in a curved path the direction of the cut through the antenna pattern will be determined by the sun's path for that time of day. At noon the sun is moving in azimuth only.

If the sun were a point source the drift curve would be the same as the antenna pattern. Since the sun has a finite diameter the antenna pattern will appear to be broader. The observed pattern broadening as a function of the source width can be calculated for a uniform source[1]. For example, if the source diameter, in degrees, equaled the half-power beam width, the broadening would be 20 percent. For the case of the Nimbus antenna with a beamwidth of 3° and a sun diameter of .54° the broadening would be 5 percent.

The absolute temperature of a uniform radio source is related to the antenna temperature by[2]:

$$T_a = T_s \left(\frac{\Omega_s}{\Omega_A}\right)$$

for $\Omega_s << \Omega_A$

where

T_A = antenna input temperature

T_s = source temperature

Ω_A = antenna beam area, rad^2

Ω_s = source solid angle, rad^2

The antenna solid angle Ω_A is related to the half-power beamwidth by[2]:

$$\Omega_A = \frac{\theta \quad \phi}{\epsilon_M}$$

where

θ = half-power beamwidth in θ plane, rad.

ϕ = half-power beamwidth in ϕ plane, rad.

ϵ_M = main beam efficiency

From the above equations we have for a circular source:

$$T_A = T_s \frac{\theta_s^2}{(\phi \ \theta)\epsilon_M}, \text{ for } \theta_s^2 << \phi\,\theta$$

where

θ_s = angular width of source

Since the dimensions of the angles cancel they may be expressed in degrees or radians.

Correcting for the atmospheric attenuation we have:

$$T_A = \frac{T_s \theta_s^2}{L(\phi\ \theta)\epsilon_M} + T_{O_2, H_2O} + T_{sky}$$

where

L = attenuation due to water vapor and oxygen

T_{sky} = total sky temperature received outside source solid angle

T_{O_2,H_2O} = temperature received due to oxygen and water vapor inside source solid angle

Figures D-1, D-2, and D-3 are sun-drift curves taken with the Nimbus antenna for Run Nos. 9, 10, and 35.

The calculated sun disk temperature and one-half power beam widths of the antenna are summarized in Table D-1.

The measured beamwidth was neither of the principal phase beamwidths because the sun drifted through a plane slightly skewed from either of these planes.

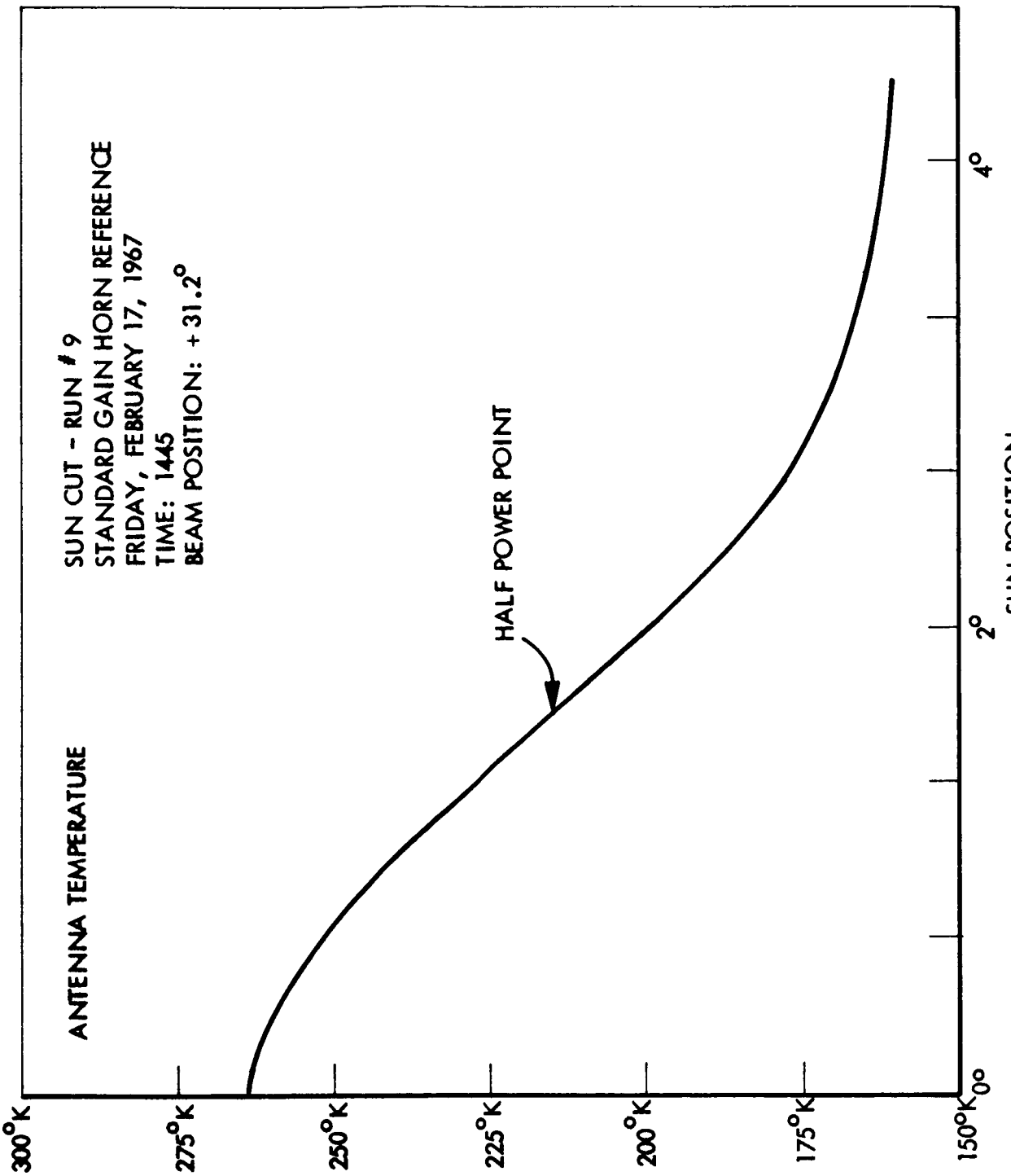

Figure D-1. Sun-Drift Curve Run No. 9

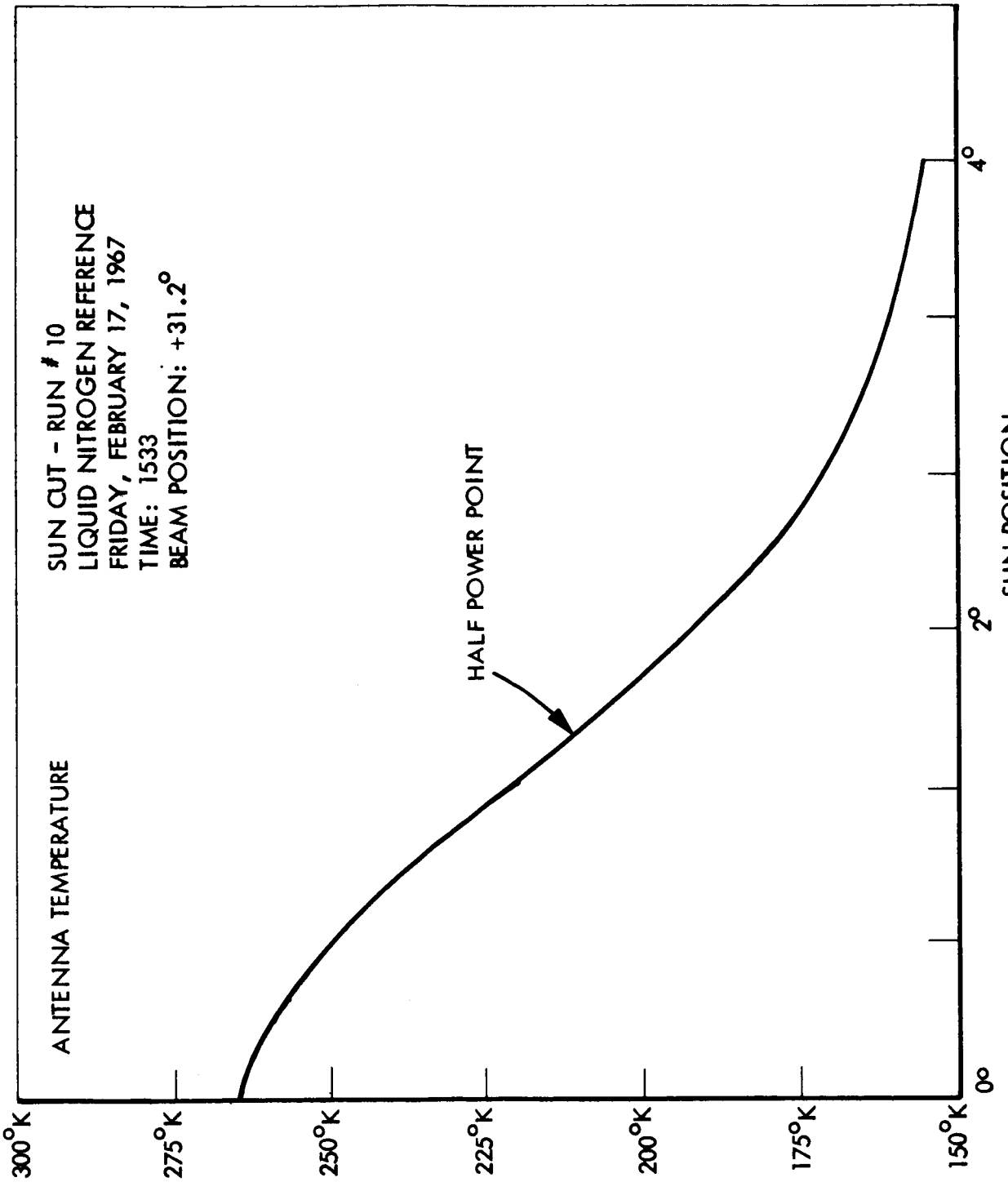

Figure D-2. Sun-Drift Curve Run No. 10

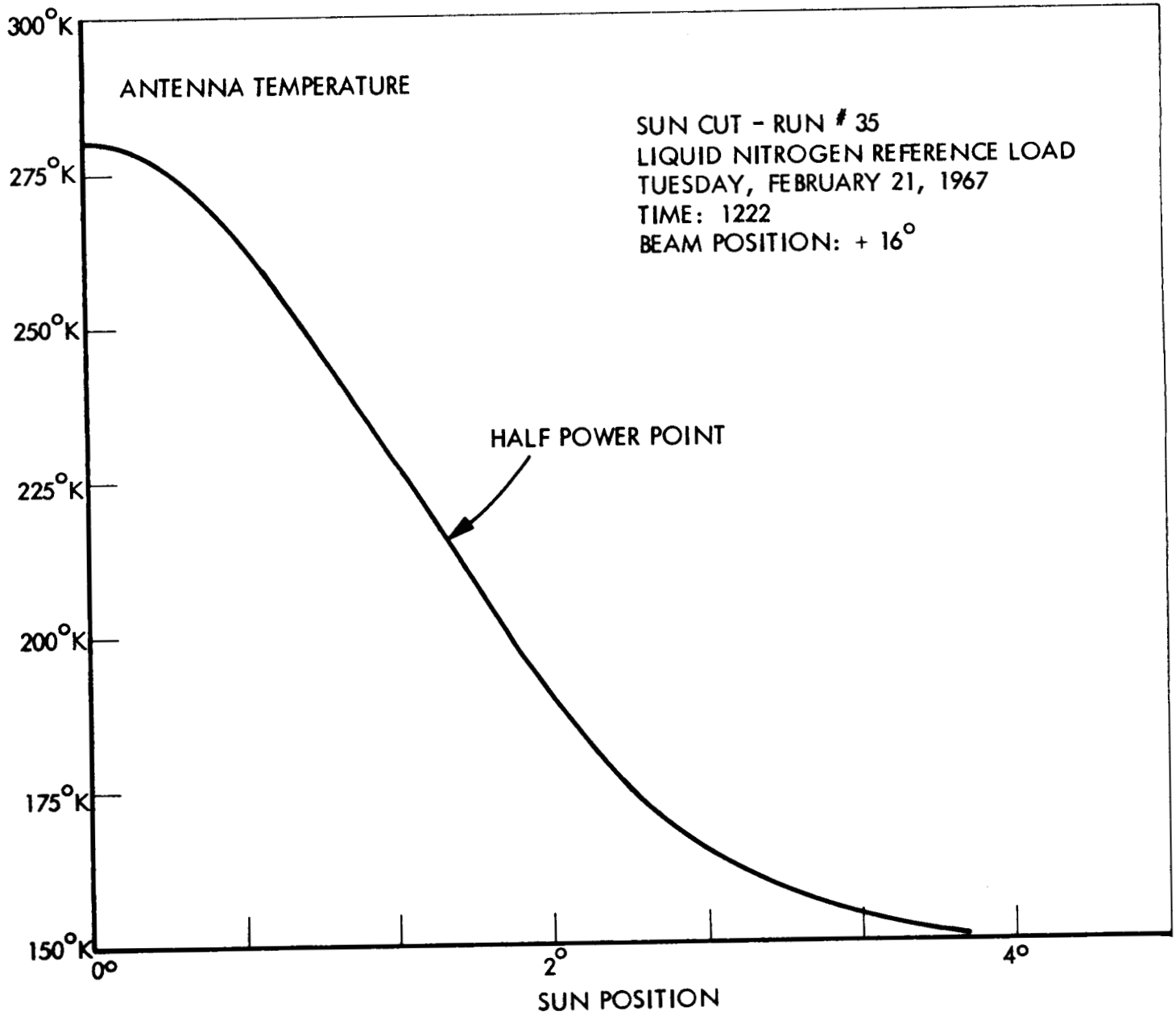

Figure D-3. Sun-Drift Curve Run No. 35

Table D-1

SUN MEASUREMENTS

Date	Time	Elevation Angle, Sun	Electrical Beam Position	Beamwidth From Sun Curve	Principal Plane Beamwidths From Antenna Range θ	Principal Plane Beamwidths From Antenna Range ∅	Measured Sun Temperature
2-21-67	1222	44°	+16°	2.91°	2.44°	2.98°	7080°K
2-17-67	1445	34°	+31.2°	3.02°	2.71°	2.98°	7160°K
2-17-67	1533	23°	+31.2°	3.04°	2.71°	2.98°	7200°K

REFERENCES

1. Kraus, J. D., Radio Astronomy, 1966, McGraw Hill, p. 171

2. Ibid, p. 72 and p. 158